PHYSICAL REVIEW D VOLUME 49, NUMBER 7 1 APRIL 1994

Comprehensive analysis of solar, atmospheric, accelerator, and reactor neutrino experiments in a hierarchical three-generation scheme

G. L. Fogli
Dipartimento di Fisica di Bari, Bari, Italy
and Istituto Nazionale di Fisica Nucleare, Sezione di Bari, Bari, Italy

E. Lisi
Dipartimento di Fisica di Bari, Bari, Italy
and Istituto Nazionale di Fisica Nucleare, Sezione di Bari, Bari, Italy
and Theory Division, CERN, Geneva, Switzerland

D. Montanino
Dipartimento di Fisica di Bari, Bari, Italy
and Istituto Nazionale di Fisica Nucleare, Sezione di Bari, Bari, Italy
(Received 13 September 1993)

We consider the possible evidence of neutrino oscillations by analyzing simultaneously, in a well-defined hierarchical three-generation scheme, all the solar and atmospheric neutrino data (except for upward-going muons) together with the constraints imposed by accelerator and reactor neutrino experiments. The analysis includes the Earth regeneration effect on solar neutrinos and the present theoretical uncertainties on solar and atmospheric neutrino fluxes. We find solutions and combined bounds in the parameter space of the neutrino masses and mixing angles, which are compatible with the whole set of experimental data and with our hierarchical assumption. We also discuss possible refinements of the analysis and the perspectives offered by the next generation of neutrino oscillation experiments.

PACS number(s): 14.60.Pq, 14.60.Lm, 96.40.Tv, 96.60.Kx

I. INTRODUCTION

Twenty years ago, neutrino physics led to the discovery of neutral currents [1], providing the first indications in favor of the electroweak standard model. At present, twenty years later, the standard model being firmly established, neutrino physics appears again as the best candidate to detect the first indications of new physics. There are, in fact, at least two experimental results concerning neutrinos that, at present, cannot be easily interpreted without requiring some effects of new physics, and the next generation of neutrino experiments is likely to provide a proof of this. They are (1) the deficit in the solar neutrino flux measured by all four existing experiments, Homestake [2], Kamiokande [3], GALLEX [4,5] and SAGE [6], probing a large part of the solar neutrino energy spectrum and (2) the low value of the ratio between ν_μ and ν_e produced in cosmic-ray interactions in the atmosphere and revealed in underground detectors.

The first discrepancy, known as the "solar neutrino problem," was discovered by the pioneering experiment of Davis [2], which is sensitive to ^{8}B and ^{7}Be neutrinos. The discrepancy was largely confirmed by Kamiokande [3], sensitive to ^{8}B neutrinos. More recently, a non-negligible neutrino deficit has been measured by GALLEX at the Gran Sasso [4,5] and SAGE in Baksan [6]. They use ^{71}Ga detectors and are sensitive, unlike earlier experiments, to the *pp* neutrinos coming from the main nuclear cycle powering the Sun. Actually, a precise theoretical estimate of the solar neutrino fluxes requires reliable models of the solar evolution up to its present luminosity. The most popular of them is the so-called standard solar model (SSM) of Bahcall and collaborators [7], in particular in its latest versions [8,9]. The SSM flux estimates have proven very robust against any upgrade of the model itself, and it appears very difficult, if not impossible, to justify the solar neutrino deficit in terms of the uncertainties affecting its parameters (as radiative opacities, nuclear cross sections, heavy-element abundance, etc.). It is then reasonable to interpret the solar neutrino deficit as a signal of new dynamical and/or kinematical properties of neutrinos. The most economical and natural solution has been proposed by Wolfenstein [10] and Mikheyev and Smirnov [11]. Known as the Mikheyev-Smirnov-Wolfenstein (MSW) effect, it assumes that neutrinos have masses and mixing angles, but no new interactions beyond the electroweak standard model. The observed neutrino deficit is attributed to matter-enhanced oscillations of the ν_e's along their way from the center of the Sun, where they are more copiously produced, to its surface. An extensive review of the subject is given in [12]. When only two neutrino families are considered, the parameter space reduces to one mixing angle and one mass-squared difference, and the allowed regions of each experiment can be drawn in the usual $(\sin^2 2\theta/\cos 2\theta, \Delta m^2)$ plane.

The second problem is the "atmospheric neutrino anomaly," which appears as a deficit in the expected ratio of ν_μ- to ν_e-induced events, observed by the two experiments which use water-Cherenkov techniques,

Kamiokande [13] and IMB [14,15]. No deficit, however, had been observed in the past by the low-statistics experiments with iron calorimeters, Fréjus [16] and NUSEX [17] (for a recent discussion of old and new data on atmospheric neutrinos, see Ref. [18]). These contradictory results may suggest large systematic errors in the two Cherenkov experiments [19] or, alternatively, some physical interpretation other than neutrino oscillation, partially supported by the uncertainties in the calculation of the absolute neutrino flux rates (no less than 20% [18]), which make the ν_μ/ν_e deficit compatible with either a ν_e excess or a ν_μ deficit. In the former case, the proton decay mode $p \to e^+ \nu\nu$ has been proposed to explain the enhancement of the rate of the single electron events of 200 to 500 MeV/c in Cherenkov detectors [20]. However, a recent experiment using an iron calorimeter (Soudan 2, [21]) also seems to indicate an atmospheric neutrino anomaly. If the anomaly consists of a ν_μ deficit, the most plausible interpretation is to suppose that μ-neutrino oscillations into other flavors take place from the production point in the atmosphere to the underground detectors, changing the relative amount of flavor-tagged events.

From the considerations reported above, it is clear that some of the experimental results on solar and atmospheric neutrinos are still controversial and require confirmation by more precise, dedicated and calibrated experiments. Moreover, the present data, even if taken at their face value, can be interpreted in different ways. However, the most natural and economical interpretation of both the solar neutrino problem and the atmospheric neutrino anomaly relies on the occurrence of oscillations between neutrinos of different flavors. In the following, we will assume the neutrino oscillation hypothesis as a matter of fact, taking into account the most updated experimental results concerning solar and atmospheric neutrinos, and verifying their compatibility with the constraints coming from accelerator and reactor neutrino oscillation experiments. This approach is seen to require the presence of (at least) three neutrino flavors, which is, on the other hand, in agreement with the SLAC [22] and CERN e^+e^- collider LEP [23] experiments. We will work in a specific three-neutrino scenario, assuming *a priori* a well-defined "mass hierarchy." As will be seen in the following, the analysis is able to provide severe bounds on the masses and mixing angles, some of these (new) bounds being strictly related to the comparison between "astrophysical" and "terrestrial" neutrinos.

The paper is organized as follows. In Sec. II we present the general framework and the simplifications assumed in the parameter space in which the three neutrino families are described. In Sec. III we report an updated analysis of the accelerator and reactor neutrino experiments, reinterpreted in a three-flavor scenario. In Sec. IV we apply the MSW description to solar neutrinos, including for the first time in a three-family scheme the Earth regeneration effect and the night-day solar neutrino rate comparison of Kamiokande [24]. In Sec. V we face the problem of the atmospheric neutrino anomaly, and estimate the ν_e- and ν_μ-induced event rates for the different experiments. To this regard, we reduce the data sample in order to adopt a simplified vacuum-oscillation description for atmospheric neutrinos. In Sec. VI we compare the information coming from the different sectors (solar, atmospheric, accelerator, and reactor neutrinos), and find bounds on masses and mixings angles in our three-generation scheme. In Sec. VII, finally, we draw our conclusions and discuss the perspectives of the future generation of experiments.

II. GENERAL FRAMEWORK

In this section we present the general framework assumed in the analysis of the different experiments, the notation adopted throughout the paper, and the simplifying assumptions that make it possible to face the problem of the three-flavor neutrino oscillations.

Let us first introduce the three-family mixing, by assuming

$$\begin{pmatrix} \nu_e \\ \nu_\mu \\ \nu_\tau \end{pmatrix} = \nu_\alpha = U_{\alpha i} \nu_i = U_{\alpha i} \begin{pmatrix} \nu_1 \\ \nu_2 \\ \nu_3 \end{pmatrix} . \tag{1}$$

In terms of Gell-Mann matrices λ_i, the 3×3 unitary matrix U, which relates in vacuum the flavor states ν_e, ν_μ, ν_τ to the mass eigenstates ν_1, ν_2, ν_3, can be expressed in the form [25]

$$U_{\alpha i} = e^{i\psi\lambda_7} \Gamma e^{i\phi\lambda_5} e^{i\omega\lambda_2} = \begin{pmatrix} 1 & 0 & 0 \\ 0 & c_\psi & s_\psi \\ 0 & -s_\psi & c_\psi \end{pmatrix} \begin{pmatrix} 1 & 0 & 0 \\ 0 & e^{i\delta} & 0 \\ 0 & 0 & e^{-i\delta} \end{pmatrix} \begin{pmatrix} c_\phi & 0 & s_\phi \\ 0 & 1 & 0 \\ -s_\phi & 0 & c_\phi \end{pmatrix} \begin{pmatrix} c_\omega & s_\omega & 0 \\ -s_\omega & c_\omega & 0 \\ 0 & 0 & 1 \end{pmatrix} . \tag{2}$$

Describing the evolution of a generic neutrino state in terms of the matrix elements $U_{\alpha i}$, the probability of the transition $\nu_\alpha \to \nu_\beta$ in vacuum after a path length L is easily derived:

$$P(\nu_\alpha \to \nu_\beta) = \left| \sum_i U^*_{\beta i} U_{\alpha i} \exp\left[-i \frac{m_i^2}{2E_\nu} L \right] \right|^2 . \tag{3}$$

Let us briefly recall some general properties of the mixing matrix and of the transition probabilities.

(1) Without loss of generality, the angles ϕ, ψ, ω can be taken to lie in the first quadrant [26].

(2) From *CPT* invariance it follows that

$$P(\nu_\alpha \to \nu_\beta) = P(\bar{\nu}_\beta \to \bar{\nu}_\alpha) . \tag{4}$$

(3) In vacuum, the *CP*-violating phase δ induces a difference between the transition probabilities of *CP*-conjugate channels. With $\Delta_{ij}=(m_i^2-m_j^2)L/2E_\nu$ it is [27,28]

$$\begin{aligned}\Delta P &= P(\nu_e\to\nu_\mu)-P(\bar\nu_e\to\bar\nu_\mu)\\ &= P(\nu_\mu\to\nu_\tau)-P(\bar\nu_\mu\to\bar\nu_\tau)\\ &= P(\nu_\tau\to\nu_e)-P(\bar\nu_\tau\to\bar\nu_e)\\ &= 4c_\phi^2 s_\phi c_\psi s_\psi c_\omega s_\omega \sin(2\delta)[\sin\Delta_{12}+\sin\Delta_{23}+\sin\Delta_{31}]\ ,\end{aligned} \tag{5}$$

the effects of mixings being separated from those of masses.

In the following, however, we will neglect the effects due to the *CP*-violating phase δ. This is certainly true for solar neutrinos, where, only $P(\nu_e\to\nu_e)$ being measured, the matrices $e^{i\psi\lambda_7}$ and Γ can be rotated away [25]. It is reasonable to neglect the *CP*-violating effects also for accelerator and reactor neutrinos, and for atmospheric neutrinos above the horizon, for which the vacuum expression (5) applies. In fact, in the right-hand side of Eq. (5), the "mixing factor" is bounded by $2/3\sqrt{3}\simeq 0.385$, whereas the "mass factor" is suppressed by the average over the E_ν spectrum (this factor is even more suppressed when L is also averaged, as is the case for atmospheric neutrinos). A further suppression effect comes from the hierarchical assumption discussed below ($m_3^2 \gg m_{1,2}^2$), which allows us to neglect the factor Δ_{12} [27].

In conclusion, *CP*-violating effects are either zero or very small, and, for our purposes, the transition probabilities in vacuum can be considered invariant with respect to particle-antiparticle exchange.

In order to further simplify the parameter space needed to describe the neutrino oscillations in a three-generation formalism, two specific assumptions are made.

(a) We assume that the three mixing angles, ϕ,ψ,ω, satisfy

$$s_\phi^2, s_\psi^2, s_\omega^2 \le \tfrac{1}{2}\ . \tag{6}$$

This is a reasonable assumption, which in general involves the dominance of the diagonal terms in the mixing matrix (2), with a rather strong correspondence between the flavor states and the mass eigenstates. In particular, the assumption has the practical consequence of establishing a one-to-one correspondence between $s_{2\theta}^2$ and s_θ^2, for all the possible cases $\theta=\phi,\psi,\omega$, when we "translate" in the three-generation scheme the results obtained in the standard two-family analyses (in which $s_{2\theta}^2$ is used).

(b) We assume a natural mass hierarchy $m_1 < m_2 < m_3$. Taking the lowest mass m_1 equal to zero for the sake of simplicity, we fix the scales of m_2 and m_3 as suggested by the most recent two-generation analyses of solar [29,30,31] and atmospheric [18] neutrinos. On the one hand, the MSW approach to the solar neutrino problem leads to $m_2^2 \simeq 10^{-5}$ eV^2, assuming $(\nu_e\leftrightarrow\nu_\mu)$ oscillations. On the other hand, the atmospheric neutrino anomaly, if interpreted in terms of $(\nu_\mu\leftrightarrow\nu_\tau)$ oscillations, requires m_3^2 of the order of 10^{-2} eV^2 or larger. Even if we expect these mass ranges to change in a full three-generation approach, we can hopefully restrict the parameter space by assuming

$$m_2^2 \le 10^{-4}\ \text{eV}^2\ ,\quad m_3^2 \ge 10^{-3}\ \text{eV}^2\ \ (m_1^2=0)\ . \tag{7}$$

This is a rather strong assumption, since we do not have *a priori* valid arguments against different choices. However, the mass hierarchy (7) is the most natural one, and the solutions we will find in the three-generation scheme (through the comparison of the experimental data on solar, atmospheric, accelerator, and reactor neutrinos) agree with it. This consistency *a posteriori* does not exclude different solutions, but guarantees that the hierarchy (7) is plausible and supported by the data.

The assumptions described above lead to some welcome simplifications in the (otherwise extremely complex) three-family picture of neutrino oscillations.

For solar neutrinos the ratios $m_2^2/2m_3^2$ and $As_{2\phi}/2m_3^2$ become small (here, as usual, $A=2\sqrt{2}G_F N_e E_\nu$ is the squared mass induced by ν interactions with background electrons of density N_e). At zeroth order in these two ratios, the 3ν problem decouples into a $2\nu\otimes 1\nu$ description, and only the first two generations experience the MSW effect [25] (see also Sec. IV).

For accelerator and reactor neutrinos, only the leading oscillation in vacuum (i.e., the fastest one, governed by high values of m_3^2) becomes relevant—an approximation known as the "one mass scale dominance" [32].

For atmospheric neutrinos, we will cut the data sample at 20° below the horizon (so reducing the maximum path length to $L=4400$ km), and adopt the vacuum oscillation approach. Once again, with typical detected neutrino energies in the range 0.2–2 GeV, and under the assumption (7), the one dominant mass scale approximation can be applied [33,34,35]. The excluded data sample might require a much more elaborate analysis (see also Sec. V).

We will find that, in the region of the parameter space allowed by present data, the neglected terms amount to a few percent at most.

In vacuum, under the one dominant mass scale approximation, the different transition probabilities of Eq. (3) can be written in the form of a symmetric matrix (valid for accelerator, reactor, and atmospheric neutrinos):

$$P\begin{bmatrix} \nu_e\to\nu_e & \nu_e\to\nu_\mu & \nu_e\to\nu_\tau \\ & \nu_\mu\to\nu_\mu & \nu_\mu\to\nu_\tau \\ & & \nu_\tau\to\nu_\tau \end{bmatrix} = \begin{bmatrix} 1-4s_\phi^2c_\phi^2S & 4s_\phi^2c_\phi^2s_\psi^2S & 4s_\phi^2c_\phi^2c_\psi^2S \\ & 1-4c_\phi^2s_\psi^2(1-c_\phi^2s_\psi^2)S & 4c_\phi^4s_\psi^2c_\psi^2S \\ & & 1-4c_\phi^2c_\psi^2(1-c_\phi^2c_\psi^2)S \end{bmatrix}\ , \tag{8}$$

where

$$S=\sin^2(m_3^2 L/4E_\nu) \tag{9}$$

depends only on the dominant squared mass m_3^2. It is important to observe that all these vacuum transition probabilities are independent of the angle ω.

III. ACCELERATOR AND REACTOR NEUTRINOS

Accelerator and reactor neutrino beams provide two complementary tools for detecting neutrino oscillations. The former are mostly μ flavored, suited to study the channels $P(\nu_\mu \to \nu_x)$ [but in one experiment, E531 at Fermilab, the small ν_e mixture is used to study $P(\nu_e \to \nu_\tau)$]. The latter are e flavored, with values of E_ν too low to study oscillations other than[1] $P(\nu_e \to \nu_e)$.

Up to now, both accelerator and reactor neutrino oscillation searches have given negative results (for a review see, for example [36]). The most constraining experiments on the various transition probabilities can be presented as follows:

$$P\begin{bmatrix} \nu_e\to\nu_e & \nu_e\to\nu_\mu & \nu_e\to\nu_\tau \\ & \nu_\mu\to\nu_\mu & \nu_\mu\to\nu_\tau \\ & & \nu_\tau\to\nu_\tau \end{bmatrix} = \begin{bmatrix} \text{Gösgen[37],IRP[38]} & \text{E776[39]} & \text{E531[40]} \\ & \text{CDHSW[41]} & \text{E531[40]} \\ & & \text{none} \end{bmatrix} \tag{10}$$

with diagonal and off-diagonal elements corresponding to the so-called "disappearance" and "appearance" experiments, respectively.

Usually, the experimental results are analyzed in terms of two-family mixing, and give constraints in the plane $(\sin^2 2\theta, \Delta m^2)$. In particular, the following expressions are customary for the transition probabilities:

$$P_{2\nu}(\nu_\alpha \to \nu_\alpha) = 1 - \sin^2 2\theta \sin^2(\Delta m^2 L/4E_\nu) ,$$
$$P_{2\nu}(\nu_\alpha \to \nu_\beta) = \sin^2 2\theta \sin^2(\Delta m^2 L/4E_\nu) , \quad \alpha \neq \beta \tag{11}$$

to be integrated over the energy spectrum and the detection cross section, in order to obtain the expected rates in the presence of oscillations. Of course, Δm^2 and θ have a different meaning for each experiment, and should be labeled by the subscripts $\alpha\beta$ (appearance of the flavor β starting from the flavor α) or αx (disappearance of the flavor α into a different, unknown, flavor x). Figure 1 collects the 90% C.L. limits provided by the various experiments (partially smoothed is the limit from Gösgen).

There are a few (old) analyses of accelerator and reactor experiments in a three-generation framework. One is Ref. [42], in which the raw data were refitted. In other papers [32,43], the one mass scale dominance was used. In this same approximation, we propose here a simple but direct reanalysis of the accelerator and reactor data. We observe that the probabilities in (8) can be generally written as

$$P_{3\nu}(\nu_\alpha \to \nu_\beta) = \delta_{\alpha\beta} - 4U_{\alpha 3}U_{\beta 3}(\delta_{\alpha\beta} - U_{\alpha 3}U_{\beta 3}) \times \sin^2(m_3^2 L/4E_\nu) , \tag{12}$$

which can be put into a one-to-one correspondence with the first of Eqs. (11) through the substitutions

$$\sin^2 2\theta \leftrightarrow 4U_{\alpha 3}U_{\beta 3}(\delta_{\alpha\beta} - U_{\alpha 3}U_{\beta 3}) ,$$
$$\Delta m^2 \leftrightarrow m_3^2 . \tag{13}$$

In particular, assuming $s_\phi^2, s_\psi^2, s_\omega^2 \leq \frac{1}{2}$ as discussed in Sec. II, we can easily work out a unique solution to the "mix-

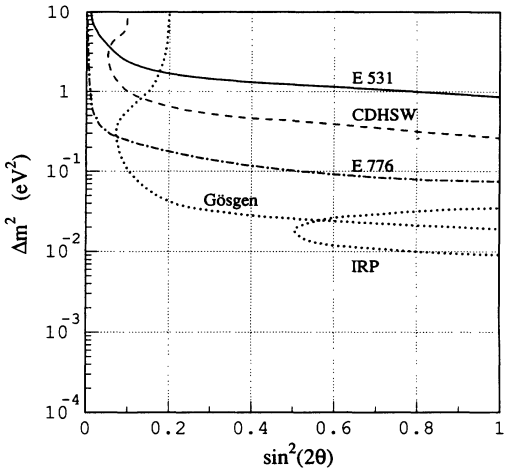

FIG. 1. Limits at the 90% C.L. on Δm^2 and $s_{2\theta}^2$, coming from accelerator and reactor experiments in the usual two-family approach. It is important to note that the limits involve two different neutrino families in each experiment, according to the following correspondence: solid line $\leftrightarrow \nu_\mu\nu_\tau$, dashed line $\leftrightarrow \nu_\mu\nu_x$, dot-dashed line $\leftrightarrow \nu_\mu\nu_e$, dotted line $\leftrightarrow \nu_e\nu_x$.

[1]Since a real mixing matrix is used (see Sec. II), no distinction is made between vacuum oscillations of neutrinos and antineutrinos, simply referred to as neutrinos in this section.

ing angle substitution" of Eq. (13) for any transition probabilities relevant to our analysis (for the $\nu_e \to \nu_\tau$ channel the present limits [40] are too weak for our purposes):

$$P(\nu_e \to \nu_e): \; s^2_{2\phi} \leftrightarrow s^2_{2\theta} \quad \text{for } 0 \le s^2_{2\theta} \le 1 \; , \tag{14a}$$

$$P(\nu_e \to \nu_\mu): \; s^2_{2\psi} \leftrightarrow 4\frac{s^2_{2\theta}}{s^2_{2\phi}}\left[1-\frac{s^2_{2\theta}}{s^2_{2\phi}}\right] \quad \text{for } 0 \le s^2_{2\theta} \le \frac{1}{2}s^2_{2\phi} \; , \tag{14b}$$

$$P(\nu_\mu \to \nu_\mu): \; s^2_{2\psi} \leftrightarrow 4\frac{s^2_\theta}{c^2_\phi}\left[1-\frac{s^2_\theta}{c^2_\phi}\right] \quad \text{for } 0 \le s^2_{2\theta} \le c^2_\phi(2-c^2_\phi) \; , \tag{14c}$$

$$P(\nu_\mu \to \nu_\tau): \; s^2_{2\psi} \leftrightarrow \frac{s^2_{2\theta}}{c^4_\phi} \quad \text{for } 0 \le s^2_{2\theta} \le c^4_\phi \; . \tag{14d}$$

Note that for reactor experiments Eq. (14a) applies, so that in this case the generic plane $(\sin^2 2\theta, \Delta m^2)$ goes into the plane $(s^2_{2\phi}, m^2_3)$. It follows that the corresponding bounds are ψ independent: for instance, given $s^2_{2\phi} \equiv s^2_{2\theta} \simeq 0.2$, the Gösgen bound is approximately $m^2_3 > 4.5 \times 10^{-2}$ eV^2 for any ψ (see Fig. 2). The ψ independence turns out to be an important feature in the comparison with the atmospheric neutrino data (see Sec. VI).

For the other channels, and for any fixed ϕ, Eqs. (14b), (14c), and (14d) make it possible to map the 90% C.L. bounds from the plane $(\sin^2 2\theta, \Delta m^2)$ to the plane $(s^2_{2\psi}, m^2_3)$. The transition probabilities, and thus the data analysis, are invariant by construction under the mapping rules described by Eqs. (13) and (14). Unfortunately, bounds at different confidence levels are not available for the quoted experiments. They should be reconstructed by using the original data on measured versus simulated events. We have not performed such a complex analysis here.

Let us, finally, point out the validity of the "one mass scale dominance" for accelerator and reactor neutrinos. Since the experiments under analysis probe values of $m^2_3 > 10^{-2}$ eV^2, the subleading oscillation, driven by $m^2_2 < 10^{-4}$ eV^2, is effectively "frozen" on the experimental length scale L, and can be safely neglected.

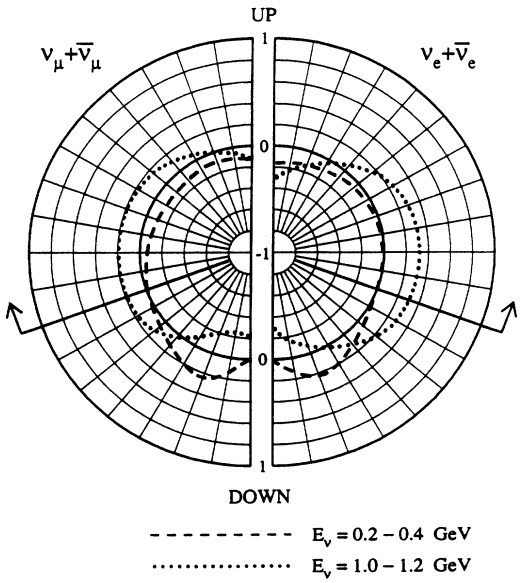

FIG. 2. Relative variation around the mean for the electron and muon (anti)neutrino fluxes at the Kamioka site, for two typical energies of the detected neutrinos, as a function of the zenith angle. Also shown are the cuts at 20° below the horizon used in our analysis (thick lines with arrows). The angular spectra anisotropy is due to geomagnetic effects and to the different thickness of the atmosphere for slanting primaries. Adapted from Ref. [55].

IV. SOLAR NEUTRINOS

The MSW analysis of the solar neutrino data for three generations, and arbitrary values of neutrino masses and mixings, is in general extremely complex. However, in some scenarios, such as the one we are using, a reduction to an "effective two-family problem" is possible.

The general 3ν-propagation problem, and the conditions under which it simplifies, have been studied by several authors [25,44,45]. In particular, we will adopt, and briefly summarize, the notation and results of Ref. [25], also used in some recent phenomenological analyses of the solar neutrino problem [46,47]. Following Ref. [25], we switch to a new "primed" basis:

$$\begin{pmatrix} \nu'_e \\ \nu'_\mu \\ \nu'_\tau \end{pmatrix} = \begin{pmatrix} c_\omega & s_\omega & 0 \\ -s_\omega & c_\omega & 0 \\ 0 & 0 & 1 \end{pmatrix} \begin{pmatrix} \nu_1 \\ \nu_2 \\ \nu_3 \end{pmatrix}$$

$$= \begin{pmatrix} c_\phi & -s_\phi s_\psi & -s_\phi c_\psi \\ 0 & c_\psi & -s_\psi \\ s_\phi & c_\phi s_\psi & c_\phi c_\psi \end{pmatrix} \begin{pmatrix} \nu_e \\ \nu_\mu \\ \nu_\tau \end{pmatrix} . \tag{15}$$

At zeroth order in $As_{2\phi}/2m^2_3$ and $m^2_2/2m^2_3$ ($A = 2\sqrt{2} G_F N_e E_\nu$), the three-family MSW evolution equations decouple into

$$i\frac{d}{dt}\begin{pmatrix} \nu'_e \\ \nu'_\mu \end{pmatrix} = \frac{1}{4E_\nu}\begin{pmatrix} -m^2_2 c_{2\omega} + Ac^2_\phi & m^2_2 s_{2\omega} \\ m^2_2 s_{2\omega} & m^2_2 c_{2\omega} - Ac^2_\phi \end{pmatrix}\begin{pmatrix} \nu'_e \\ \nu'_\mu \end{pmatrix} ,$$

$$i\frac{d}{dt}\nu'_\tau = \frac{m^2_3}{2E_\nu}\nu'_\tau \; . \tag{16}$$

In this case, it is customary to say that only the "lower resonance" is effective, since the matter-induced mass term Ac^2_ϕ can, at most, make the effective masses $(m^2_1)_{\text{matter}}$ and $(m^2_2)_{\text{matter}}$ degenerate, whilst $(m^2_3)_{\text{matter}} \simeq m^2_3$ and $(\phi)_{\text{matter}} \simeq \phi$. In particular, for $E_\nu \simeq 10$ MeV, at the center of the Sun $A \simeq 1.5 \times 10^{-4}$ eV^2, so that in our assumed mass hierarchy $As_{2\phi}/2m^2_3$ and $m^2_2/2m^2_3$ are less than $\frac{1}{10}$, or even lower. Note also that the first of Eqs. (16) is equivalent to the standard 2ν evolution equation with the substitution $\nu \to \nu'$ and

$A \to A c_\phi^2$ (i.e., $N_e \to N_e c_\phi^2$).

Let us now describe the evolution of solar neutrinos. The starting neutrino state in the Sun is

$$|\nu\rangle_0 = |\nu_e\rangle = s_\phi |\nu_3\rangle + c_\phi |\nu'_e\rangle \ . \tag{17}$$

The evolution of $|\nu_3\rangle$ is trivial,

$$|\nu_3\rangle \to \exp\left[-i\frac{m_3^2}{2E_\nu}t\right]|\nu_3\rangle \ , \tag{18}$$

but the evolution of $|\nu'_e\rangle$ can be obtained only by solving Eq. (16) (semianalytically in the Sun and numerically in the Earth) in terms of the 2ν transition amplitudes. We have

$$|\nu'_e\rangle \to T_{2\nu}(\nu'_e \to \nu'_e)|\nu'_e\rangle + T_{2\nu}(\nu'_e \to \nu'_\mu)|\nu'_\mu\rangle \ , \tag{19}$$

leading to the final neutrino state at the time t:

$$|\nu\rangle_t = \exp\left[-i\frac{m_3^2}{2E_\nu}t\right] s_\phi |\nu_3\rangle + T_{2\nu}(\nu'_e \to \nu'_e) c_\phi |\nu'_e\rangle + T_{2\nu}(\nu'_e \to \nu'_\mu) c_\phi |\nu'_\mu\rangle \ . \tag{20}$$

In conclusion, the detection amplitude of $|\nu_e\rangle$ in $|\nu\rangle_t$ is

$$\begin{aligned} T_{3\nu}(\nu_e \to \nu_e)\langle \nu_e|\nu\rangle_t &= s_\phi \exp\left[-i\frac{m_3^2}{2E_\nu}t\right]\langle \nu_e|\nu_3\rangle + c_\phi T_{2\nu}(\nu'_e \to \nu'_e)\langle \nu_e|\nu'_e\rangle + c_\phi T_{2\nu}(\nu'_e \to \nu'_\mu)\langle \nu_e|\nu'_\mu\rangle \\ &= s_\phi^2 \exp\left[-i\frac{m_3^2}{2E_\nu}t\right] + c_\phi^2 T_{2\nu}(\nu'_e \to \nu'_e) \ . \end{aligned} \tag{21}$$

Taking the squared modulus, and then averaging out the interference term:

$$P_{3\nu}(\nu_e \to \nu_e) = s_\phi^4 + c_\phi^4 P_{2\nu}(\nu'_e \to \nu'_e) \ , \tag{22}$$

where we remark that $P_{2\nu}$ is calculated as in the two-family case, provided that $N_e \to N_e c_\phi^2$ (see also the first of Refs. [47]).

This lower "effective density" and the factor c_ϕ^4 tend to reduce the MSW effects in $P_{3\nu}$. As a consequence, the iso-SNU (solar neutrino unit) lines in the mass-mixing plane turn out to be more spaced, and the regions allowed by each single experimental result enlarged (see Sec. VI). Notice also that, for any fixed ϕ, the probability $P_{3\nu}$ depends only on m_2^2 and ω.

As was said before, Eq. (16) can be solved semianalytically inside the Sun. We take from Refs. [8,9] the eight relevant neutrino fluxes, the spatial distribution of the neutrino sources and the electron density profile in the Sun. Moreover, from the same works we adopt the single components of the estimated astrophysical errors, and the matrix of logarithmic derivatives linking them to the flux errors. For each value of ϕ, m_2^2, and ω, we propagate these uncertainties to the final SNU predicted for each experiment. The final theoretical errors affecting the different experiments are then correlated, and are added to the uncorrelated statistical and systematic errors (see also [31]).

Along their way toward the detectors, neutrinos are eventually affected by the Earth's matter. The Earth regeneration effect bends the iso-SNU curves at large angles, and induces an asymmetry between the averaged night (N) and day (D) expected rates. Quantitative estimates require a reliable model of the Earth's radial density [48], and have been carried out, for two families of neutrinos, by several authors [49–52]. Recent applications are contained in [53,54].

In this paper we incorporate, for the first time, the Earth regeneration effect on the iso-SNU curves and on the night-day flux asymmetry [defined as $(N-D)/(N+D)$] in a three-generation scenario. In order to reduce the computational effort, we assume a constant density in each of the five shells identified in [48] along the Earth's radius (inner core, outer core, lower mantle, transition zone, upper mantle). Along a single neutrino trajectory, the resulting transition probability can be appreciably different with respect to a full Earth-density-profile treatment, but when sums over trajectories are performed to obtain yearly averages, the differences turn out to be very small. A similar approach has been adopted in Ref. [54].

The data on the solar neutrino fluxes we use in the analysis are the most recent average rates measured by the four existing experiments Homestake [2], Kamiokande [3], GALLEX [4,5], and SAGE [6], and are summarized in Table I, normalized to the corresponding SSM expected rates [9]. In particular, the preliminary data of Kamiokande III and GALLEX II [5] are also included. The solar neutrino data are completed with the measurement of the $N-D$ asymmetry (whose value is compatible with zero), performed by Kamiokande [24]:

$$\frac{N-D}{N+D} = 0.08 \pm 0.11(\text{stat}) \pm 0.03(\text{syst}) \ . \tag{23}$$

Concerning this measurement, we do not use the further information given by the data binning in the zenith angle. The results of our solar neutrino analysis are discussed in Sec. VI.

V. ATMOSPHERIC NEUTRINOS

Neutrinos produced in the atmosphere by cosmic primary collisions (and subsequent decays) can trigger two

TABLE I. Data of the four solar neutrino experiments. The comparison with the standard solar model (SSM) makes use of the last version of the Bahcall SSM [9]. The third error in the column (Data/SSM) refers to the total theoretical uncertainty affecting the SSM, as discussed in [8] and [9].

Experiment	Ref.	Relative flux (data/SSM)
Homestake (^{37}Cl)	[2]	$0.27\pm0.04(\text{expt})\pm0.03(\text{theor})$
Kamiokande (water)[a]	[3]	$0.50\pm0.05(\text{stat})\pm0.06(\text{syst})\pm0.07(\text{theor})$
GALLEX I+II(^{71}Ga)	[4,5]	$0.66\pm0.11(\text{stat})\pm0.05(\text{syst})\pm0.03(\text{theor})$
SAGE (^{71}Ga)	[6]	$0.44^{+0.13}_{-0.18}(\text{stat})\pm0.11(\text{syst})\pm0.02(\text{theor})$

[a]Kamiokande data are a combination of the final result of Kamiokande II (1040 days) with the measurement of Kamiokande III (220 days, preliminary).

kinds of events in underground detectors: (i) events with the primary vertex inside the fiducial volume ("contained" events); (ii) events with the primary vertex in the rock below the detector ("upward-going muon" events).

In both cases the measured rates must be compared with a detailed Monte Carlo simulation or with semi-analytical predictions of the atmospheric neutrino fluxes.

In the energy range of interest for case (i), $E_\nu = 0.1-2$ GeV, several calculations of the different e-like, μ-like, neutrino, and antineutrino fluxes are available [55–57], all including the μ-polarization effect [58]. However, the different absolute estimates may disagree as much as 30%, and this uncertainty could even be underestimated [59]. Conversely, the expected *ratio* $R^0_{\mu/e}$ of $(\nu_\mu+\bar{\nu}_\mu)$- to $(\nu_e+\bar{\nu}_e)$-induced events seems to be more stable. Thus, it is useful to express the data as a double ratio $R_{\mu/e}/R^0_{\mu/e}$ of experimental-to-theoretical μ-like to e-like events. A maximum theoretical 5% uncertainty is generally quoted in this case.

In case (ii), of course, one cannot take advantage of the error cancellation in the μ/e ratio, because only μ-like events can be detected. The measured muon rates in Baksan [60], Kamiokande [61], and IMB [62] seem to be in conflict with an oscillatory scenario (at least in a simplified two-family approach [18]). However, this interpretation is heavily dependent on the adopted neutrino flux estimates and on the assumed uncertainties [59,63].

The analysis of three-flavor oscillations in the lower hemisphere (respect to the detector) requires the inclusion of the MSW effects in the Earth. This would be a minor complication, should matter effects preserve the "one dominant mass scale" approximation. Conversely, if the subleading oscillation were enhanced in a non-negligible way, a fully general 3ν formalism and a much more refined analysis would be needed. The study of this topic is beyond the scope of this paper and deserves a separate work. Actually, the analysis in Ref. [64] (performed in two flavors only) show that values of Δm^2 in the range from 10^{-4} to 10^{-3} eV^2 are required to get MSW effects larger than 10%, at least for contained events. A naïve generalization to our hierarchical scenario (7) could therefore suggest mild changes with respect to an "empty Earth" approach, as used in Refs. [33–35]. In absence of a full check of this hint, it is safer to study only neutrino oscillations in vacuum, where the subleading oscillation contributes negligibly.

On the basis of the previous considerations, we decide to exclude muon data from this analysis, and focus our attention only on "contained" events induced by downward-going neutrinos. More precisely, we cut the data sample at 20° below the horizon, where MSW effects in the Earth start being non-negligible [64], and use the vacuum transition probabilities of Eq. (8). The resulting loss in statistics does not increase dramatically the total experimental error, since the systematic errors are left unchanged. An unavoidable loss of sensitivity to low values of m^2_3 is induced by the reduction of the average path length with respect to a full solid angle integration. Concerning the experimental data set, we are forced to abandon the (very low statistics) NUSEX data [17], for which no up and/or down distinction is possible. The preliminary Soudan 2 results [21] are not included either, because a detailed publication of the data and of their treatment is still lacking.

We adopt, in the following, the spectra in the zenith angle and in the neutrino and antineutrino energy as calculated by Gaisser and collaborators [55] for each detector site. A graphical representation of a typical atmospheric neutrino and antineutrino sky is shown in Fig. 2, together with the angular cuts we use.

Atmospheric neutrinos undergo charged-current (CC) or neutral-current (NC) interactions in the detectors. However, the data samples we select contain mainly, or only, CC events. In the energy range $E_\nu = 0.1-2$ GeV, the dominant CC process is the quasielastic (QE) scattering of neutrinos off free or bound nucleons [65]. In the latter case, the cross section must be weighted by a final-state Pauli-blocking correction [65,66]. The subdominant process is the one-pion (1π) production [67] at the $\Delta(1234)$ resonance. In Cherenkov detectors, 1π processes can produce a second photon ring, in addition to that produced by the final-state lepton, and this happens about half of the times. Since only single-ring (SR) events are selected in the Kamiokande and IMB analyses, the 1π cross section must be weighted by a factor of about $\frac{1}{2}$ (see also [68]). The weight is 1 for the Fréjus experiment, whose detector is an iron calorimeter. We neglect the small contributions due to multipion production and NC contamination, and fold the total cross section (QE+1π) with the published efficiencies, within the experimental cuts [14,16,69].

Finally, we integrate over the neutrino and antineutrino spectra, taking into account the total exposure of the detectors (usually expressed in kton yr). In the Fréjus

TABLE II. Experimental values of the double ratio $R_{\mu/e}/R^0_{\mu/e}$, using the fluxes of Refs. [55], and their theoretical errors.

Experiment	Exposure (kton yr)	$R_{\mu/e}/R^0_{\mu/e}$	Cuts in e-like events (GeV)	Cuts in μ-like events (GeV)	Cuts in zenith angle
Kamiokande	4.92	0.60±0.07(stat)±0.05(syst)	$0.1 \le p_e \le 1.33$	$0.2 \le p_\mu \le 1.50$	None
IMB	7.70	0.55±0.05(stat)±0.10(syst)	$0.1 \le p_e \le 1.50$	$0.3 \le p_\mu \le 1.50$	None
Fréjus	1.56	1.06±0.18(stat)±0.15(syst)	$E_e \ge 0.2$	$E_\mu \ge 0.2$	None

spectra, the neutrino energy has been identified with the published "visible energy" of the ν-induced event [16]. As a result, we are able to reproduce accurately, and *without any normalization,* the Monte Carlo estimated rates of Kamiokande, IMB, and Fréjus, as shown in Fig. 3. In the same figure, the "bump" in the Fréjus curves is due to the onset of the 1π production. The "bump" is absent from the IMB and Kamiokande curves, since the lepton momentum spectra of QE and 1π processes are similar.

Confident in our treatment of the ν interactions in the detectors, we now discuss the starting data sample. In Table II we summarize the μ/e ratios measured by Kamiokande, IMB, and Fréjus, normalized to the expected μ/e ratio according to the Gaisser fluxes [55].

A few remarks are in order to explain the small differences that can be found in Table II with respect to the published values.

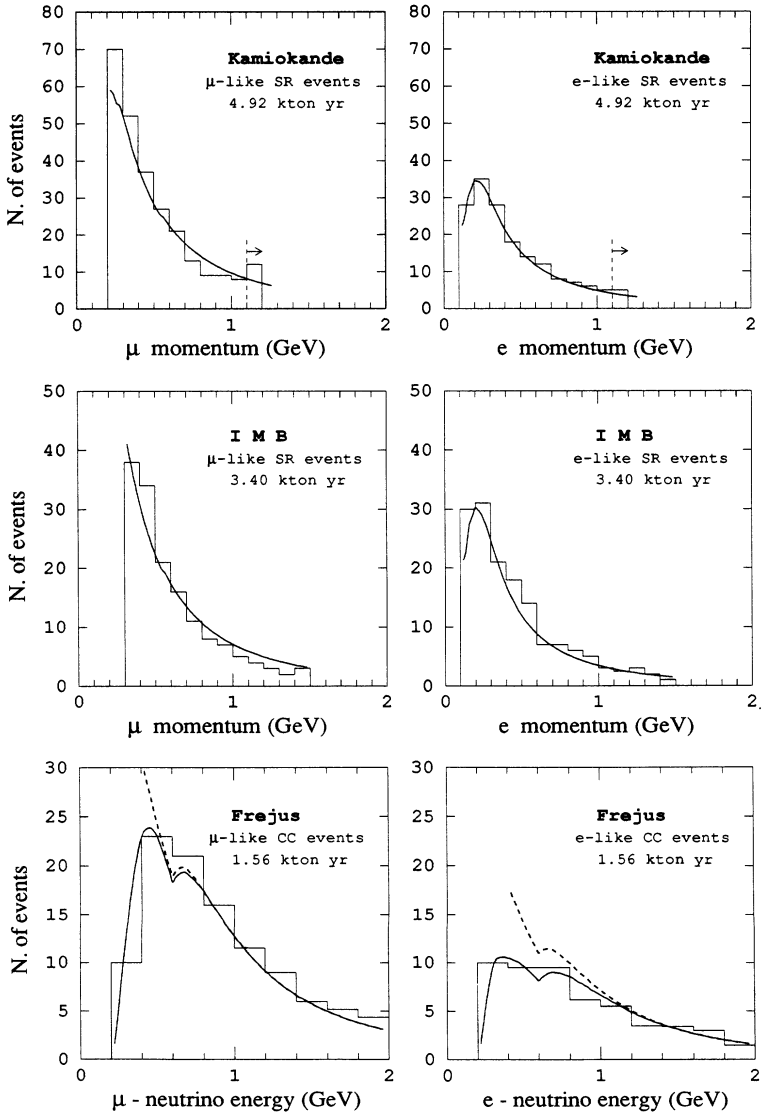

FIG. 3. Comparison between our calculation of the atmospheric neutrino events and the Monte Carlo estimate for ν_μ-induced and ν_e-induced single ring (SR) events in Kamiokande and IMB, and charged-current (CC) events in Fréjus, for given exposures of the detectors. Histograms: Monte Carlo estimates, as reported in [70,16], using the fluxes of Gaisser and collaborators [55]. Solid lines: our calculations, using the same fluxes and the published detector efficiencies. For Kamiokande and IMB the efficiencies can be safely considered constant with energy, within the kinematical cuts. For Fréjus this approximation would give the wrong result, indicated by the dashed line. Notice that the comparison is absolute, i.e., no normalization of the curves has been introduced.

(1) The statistical error of the Kamiokande result [13] has been symmetrized. (2) The IMB collaboration uses by default the fluxes of Ref. [57]. Thus, the double ratio of Table II for IMB has been obtained by dividing the μ/e ratio taken from the most recent IMB data [15] by the corresponding Monte Carlo ratio using the Gaisser fluxes, as given in [14]. For the total systematic error of IMB, we adopt the 18% estimate given in [70], obtained by adding the single systematic errors in quadrature. (3) For the Fréjus experiment we use the so-called "all CC events" sample given in Ref. [16], adding a total systematic error of 14%, as estimated in [18]. (4) In all three experiments, the systematic errors include a 5% component due to the neutrino flux uncertainties in the Monte Carlo μ/e ratio.

In our approach, however, we cannot use the results reported in Table II as they stand. As explained before, in order to safely use the vacuum oscillation treatment for the atmospheric neutrinos, we cut the neutrino direction at 20° below the horizon or, equivalently, we take $\cos\theta_z \geq -0.35$, θ_z being the zenith angle.

For each experiment, the published angular distribution of the recorded events is given in five bins, equally dividing the interval $-1 \leq \cos\theta_z \leq +1$ (care must be taken here since the IMB collaboration uses the opposite sign convention and assumes $\cos\theta_z = +1$ for neutrinos coming from below). Our cut can be implemented assigning weight zero to the bin $(-1.0, -0.6)$, weight $\frac{3}{8}$ to the bin $(-0.6, -0.2)$, and weight 1 to the other three bins.

We also include a cut for the neutrino energy in the treatment of the Fréjus data: $E_\nu \leq 2$ GeV. In fact, above this energy the multipion production and the deep inelastic scattering of neutrinos, which we have neglected, give an increasingly important contribution to the total cross section. With this cut, 19 CC μ-like events and 16 CC e-like events are lost in the data sample, and 20 and 21 events in the corresponding Monte Carlo histograms (see [16]). Since the Fréjus data sample is in agreement with the Monte Carlo expectations, we assume, in the absence of any other information, that the angular distribution of these lost events follows the theoretical one, as predicted by [55] for $E_\nu > 2$ GeV at Fréjus.

Finally, we extract the 5% flux error out of the total systematic error for each experiment, because our unified treatment of the neutrino fluxes allows us to include it at the end as a common systematic error of the three experiments. This treatment of the theoretical flux errors is a very peculiar feature of our analysis of the atmospheric neutrinos, and is likely to become even more important in the future. In fact, not only the statistical errors but also the experimental systematic errors are expected to be reduced in the IMB and Kamiokande experiments. When all the above cuts are applied, Table II takes the form reported in Table III.

Table III represents our experimental input for the three-flavor oscillation analysis. More precisely, for each experiment the experimental double ratio reported in Table III must be compared with the theoretical one, estimated in the presence of vacuum oscillations. In the one dominant mass scale approximation, the oscillatory behavior is governed by three parameters: m_3^2, ϕ, and ψ [see Eq. (8)]. We choose to fix ϕ, and study the theoretical values of the double ratio $R_{\mu/e}/R_{\mu/e}^0$ in the plane $(s_{2\psi}^2, m_3^2)$.

In order to obtain the theoretical value of $R_{\mu/e}$, the transition probabilities [multiplied by the interaction differential cross section, the detector efficiencies, and the atmospheric (anti)neutrino energy and angular spectra] must be integrated over the three variables represented by the final lepton energy, the initial neutrino energy, and the zenith angle (within the given cuts). A similar approach is followed, for instance, in Refs. [33–35]. We have checked, as in [33], that a further integration over the height distribution of the neutrinos produced in the atmosphere would produce negligible changes in our results. Therefore, we fix the production layer at a conventional 15 km height.

Through the approach described above, we derive the iso-double-ratio curves in the plane $(s_{2\psi}^2, m_3^2)$, which we will discuss thoroughly in Sec. VI. We anticipate here only one feature, to justify our choice of showing these curves for m_3^2 as low as 10^{-4} eV^2 [that is, below the limit assumed in (7)]. For such low values of the third neutrino mass, the theoretical double ratio $R_{\mu/e}/R_{\mu/e}^0$ differs from unity by at most a few percent. This means that for a mass $m^2 < 10^4$ eV^2 an oscillatory term of the type $S = \sin^2(m^2 L/4E_\nu)$ produces (averaged in the triple integral) a very small variation of $R_{\mu/e}$ with respect to the no-oscillation result $R_{\mu/e}^0$. Thus, if m_2^2 and m_3^2 satisfy the assumption (7), the subdominant oscillation (driven by m_2^2) is safely negligible in vacuum with respect to the dominant one (driven by m_3^2). Moreover, we will find in the next section that the solar and atmospheric neutrino data constrain the two masses well within the limits adopted in (7). We can conclude that (i) the "one mass scale dominance" is indeed a consistent description for the atmospheric neutrinos, and (ii) the high scale of m_3^2 ensures that at the lowest order the decoupling $3\nu \to 2\nu \otimes 1\nu$ applies for solar neutrinos.

TABLE III. Experimental values of the double ratio $R_{\mu/e}/R_{\mu/e}^0$, with the introduction of the cuts discussed in the text and using the Gaisser fluxes [55], without their theoretical errors.

Experiment	Exposure (kton yr)	$R_{\mu/e}/R_{\mu/e}^0$	Cuts in e-like events (in GeV)	Cuts in μ-like events (in GeV)	Cuts in $\cos\theta_x$
Kamiokande	4.92	$0.59 \pm 0.09(\text{stat}) \pm 0.035(\text{syst})$	$0.1 \leq p_e \leq 1.33$	$0.2 \leq p_\mu \leq 1.5$	≥ -0.35
IMB	7.70	$0.51 \pm 0.06(\text{stat}) \pm 0.095(\text{syst})$	$0.1 \leq p_e \leq 1.50$	$0.3 \leq p_\mu \leq 1.5$	≥ -0.35
Fréjus	1.56	$1.14 \pm 0.22(\text{stat}) \pm 0.150(\text{syst})$	$E_\nu \leq 2; E_e \geq 0.2$	$E_\nu \leq 2; E_\mu \geq 0.2$	≥ -0.35

VI. BOUNDS ON MASSES AND MIXINGS

In Sec. II we have set to zero both m_1^2 and δ. It follows that the variables describing the global parameter space reduce to $(m_2^2, m_3^2, \omega, \phi, \psi)$. As explained in the previous sections, solar neutrino oscillations are described in the subspace (m_2^2, ω, ϕ), while atmospheric, reactor, and accelerator neutrino oscillations in the subspace (m_3^2, ψ, ϕ). We choose to fix ϕ at three representative values, $s_\phi^2 = 0$, 0.1, 0.25, in order to decouple these two subspaces to the familiar planes $(s_{2\omega}^2/c_{2\omega}, m_2^2)$, $(s_{2\psi}^2, m_3^2)$.

The two planes are scanned by an 80×80 and a 40×40 grid of points, respectively. The two squared masses are made to range 1 order of magnitude outside the limits assumed in (7), in order to appreciate the validity of our assumptions. At each grid point, a χ^2 analysis is performed on the solar and atmospheric neutrino data, with and without the inclusion of the theoretical uncertainties related to the standard solar model and the atmospheric neutrino flux estimates. We remark that the inclusion of these theoretical errors generates off-diagonal terms in the total covariance matrix, and that for the first time they are treated in the proper way in the analysis of atmospheric neutrinos–i.e., as common systematics.

As explained in Sec. III, we do not analyze the raw data of the accelerator and reactor neutrino oscillation experiments, but simply map the 90% C.L. published bounds on the plane $(s_{2\psi}^2, m_3^2)$ for each given ϕ. When comparing in the same plane atmospheric with accelerator and reactor limits, one should be aware that the format of the latter is not χ^2-like.

In the following, we discuss in detail the results of this comprehensive analysis, in the three cases corresponding to the selected values of ϕ. Since there is considerable debate about the estimate of both the theoretical and the experimental errors, we present the final results at four different, from 1σ to 4σ, confidence levels.

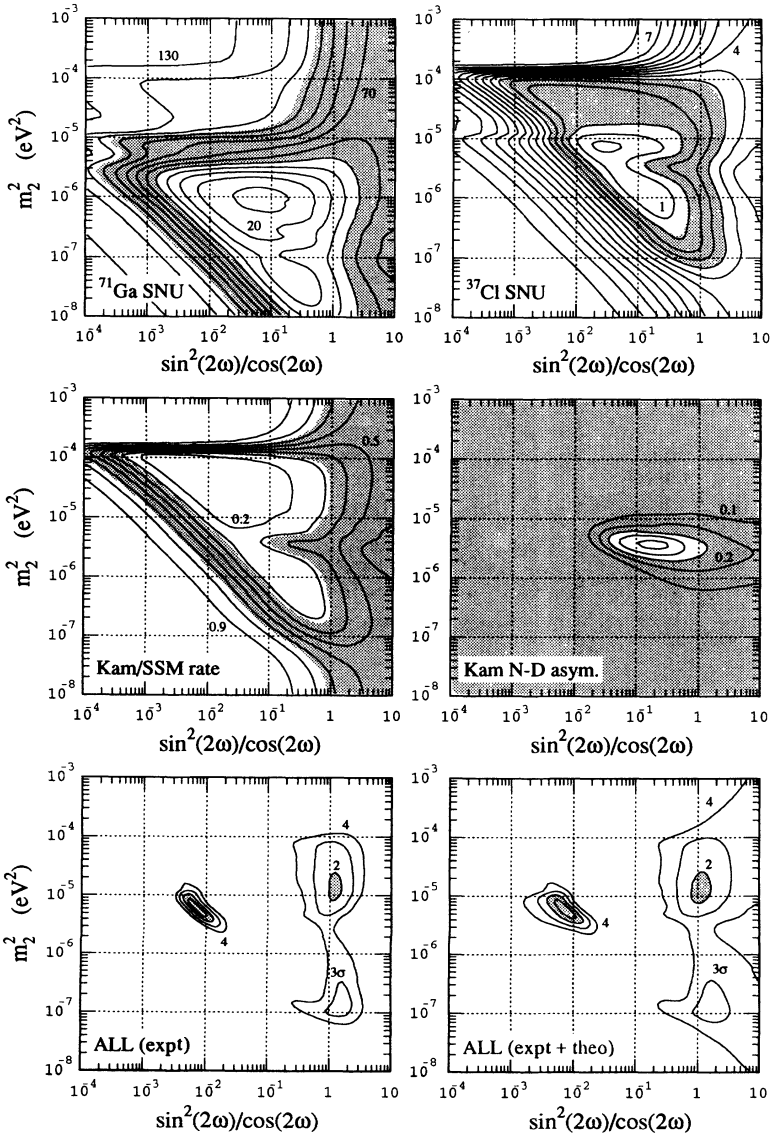

FIG. 4. MSW solutions to the solar neutrino problem for $s_\phi^2 = 0$. The grey areas, allowed at the 2σ level, refer to each experiment separately in the upper four subfigures, and to their combination in the lower two (ALL). See the text for details.

A. $\sin^2\phi=0$

For $\phi=0$, the solar and atmospheric neutrino problems are completely decoupled. The probability $P_{3\nu}(\nu_e\to\nu_e)$ for solar neutrinos in Eq. (22) reduces to the usual two-family expression $P_{2\nu}$ for $(\nu_e\leftrightarrow\nu_\mu)$ oscillations, and the matrix probability of Eq. (8) reduces to the 2×2 $(\nu_\mu\leftrightarrow\nu_\tau)$ submatrix. In this case, therefore, we can refer directly to the standard two-family analyzes.

In Fig. 4 we show the MSW solutions to the solar neutrino problem in the plane $(s^2_{2\omega}/c_{2\omega}, m^2_2)$. The first four subfigures, ^{71}Ga, ^{37}Cl, Kam, and Kam $N-D$ asym, correspond to GALLEX+SAGE, Homestake, the average Kamiokande rate, and the Kamiokande $(N-D/N+D)$ asymmetry, respectively. Solid lines represent, as usual, iso-SNU or isorate curves. The grey areas are allowed at the 2σ level by the experimental data, including theoretical uncertainties (which cancel out in the ratio $N-D/N+D$). The iso-SNU curves are bent by the Earth regeneration effect at large angles and intermediate mass values. However, that zone is mostly excluded by the $N-D/N+D$ measurement, largely compatible with zero. The data are combined in the last two subfigures (ALL), taking into account experimental (expt) and total (expt+theo) errors. In ALL, the solid lines represent iso-standard-deviation contours, for $\sigma=1,2,3,4$ (i.e., $\Delta\chi^2=1,4,9,16$). At 2σ, a "small-angle" and a "large-angle" solution can be clearly distinguished. For the small-angle solution, we find $\chi^2=0.70$ (0.69) without (with) the inclusion of the theoretical errors. For the, disfavoured, large-angle solution, it is $\chi^2=3.9$ (3.6). It can be noticed that the minimum χ^2 values are not appreciably affected by the inclusion of the theoretical errors, but the contours of the allowed regions are. At 3σ, a third solution appears at large angles and low m^2_2. It would merge into the previous large-angle solution if Earth's effects were excluded.

In Fig. 5, drawn in the plane $(s^2_{2\psi}, m^2_3)$, we show the vacuum oscillation solutions to the atmospheric neutrino deficit and their compatibility with accelerator and reac-

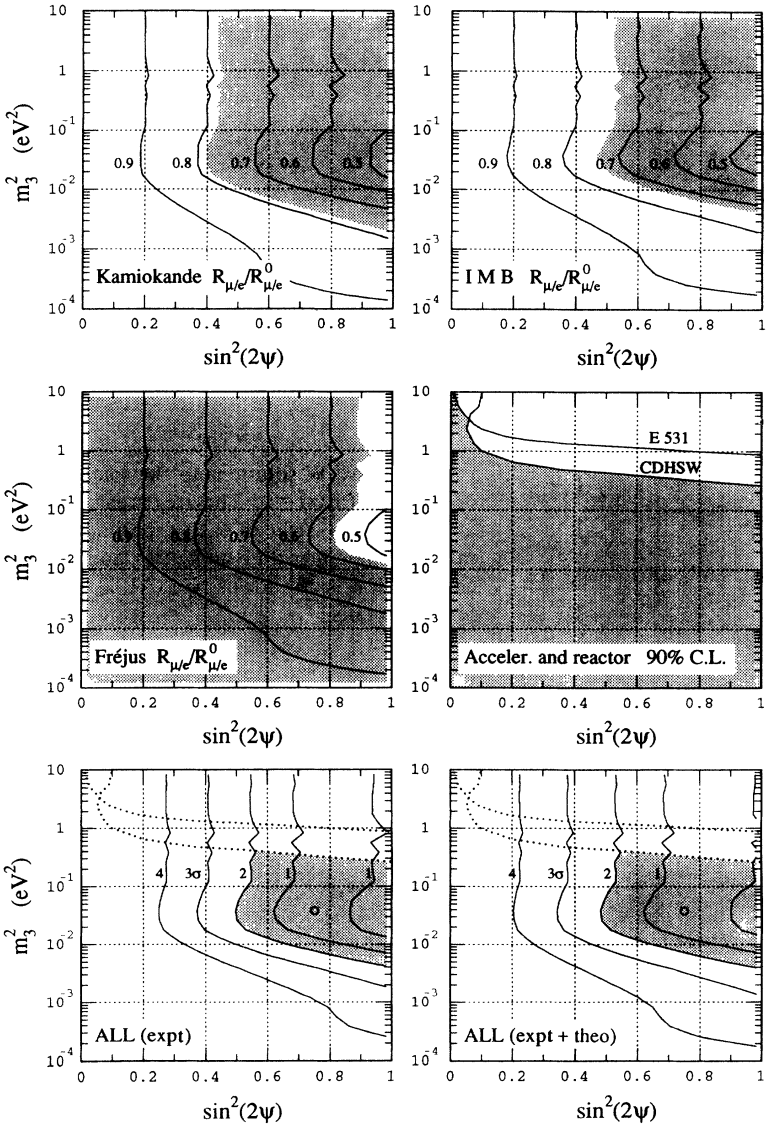

FIG. 5. Vacuum oscillation solutions to the atmospheric neutrino deficit for $s^2_\phi=0$, compared with the accelerator and reactor limits. The grey areas are allowed at the 2σ level (or 90%, where indicated). The combined bounds are shown in the last two subfigures (ALL). See the text for details.

tor neutrino data. In the first three subfigures, labeled Kamiokande, IMB, and Fréjus, we report the equally spaced iso-$(R_{\mu/e}/R^0_{\mu/e})$ curves for the corresponding experiments. Their "wavy" behavior for $m_3^2 > 10^{-1}$ eV^2 is largely due to finite-size effects of the 40×40 grid used. The grey areas cover the 2σ allowed regions, including the theoretical uncertainties. Our limits appear larger than those usually reported in the literature for $(\nu_\mu \to \nu_e)$ oscillations [13,71], because we use a reduced data sample (see Sec. V). In the subfigure "acceler. and reactor," only the E531 and CDHSW bounds are mapped onto the $(s^2_{2\psi}, m^2_3)$ plane, since E776, IRP, and Gösgen give no limits at $\phi=0$ [see Eqs. (14) and Fig. 1]. Here the grey area is simply a superposition of the regions allowed at the 90% C.L. by the quoted experiments. In the last two subfigures, the above results are combined, without [ALL(expt)] and with [ALL(expt+theo)] the theoretical uncertainties affecting the neutrino flux estimate. Notice that the limits from accelerator and reactor experiments (redrawn as dotted lines) have a fixed 90% C.L., whilst for the iso-σ contours (corresponding to the atmospheric data fit) the C.L. is variable. The upper limits on m_3^2 arise from the combination of these two data sets. It is evident that the high-statistics IMB and Kamiokande experiments dominate the atmospheric data fit. The discrepancy with the Fréjus results shows up as a relatively high value of the "atmospheric" χ^2 at the minima (the small circles in the picture): $\chi^2=4.59$ (4.57) without (with) the theoretical errors. The minimum solar+atmospheric χ^2 is thus 5.29 (5.26).

Let us remark that in Figs. 4 and 5 our starting hypothesis (7) is satisfied at the 3σ level, as anticipated in the previous sections.

B. $\sin^2\phi=0.1$

This case is representative of an "intermediate" mixing between the first and the third generations, a situation that requires a full three-generation approach.

Figure 6, if compared with Fig. 4, shows a general "ex-

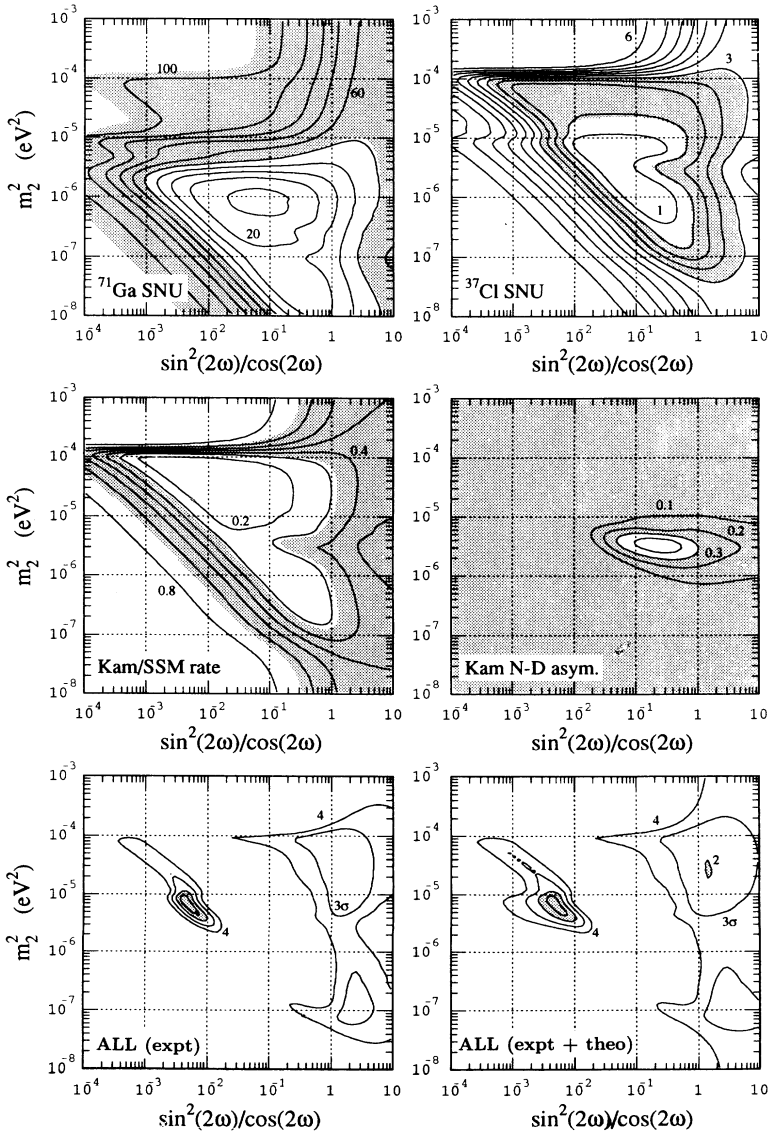

FIG. 6. As in Fig. 4, but for $s^2_\phi=0.1$.

pansion" of the triangle-shaped solutions for the gallium, chlorine, and Kamiokande experiments, as a result of the effective weakening of the MSW effect (see Sec. IV). For the same reason, the $N-D$ asymmetry data exclude a (slightly) smaller region. When the data are combined together, the small-angle and the large-angle solutions are both enlarged at the 3σ and 4σ levels. However, at the 2σ level the large-angle solution appears only when theoretical uncertainties are included. Compared with the $\phi=0$ case, higher values of m_2^2 are now allowed. The χ^2 value at the absolute minimum, located within the small-angle solution, is 1.48 (1.32) without (with) the inclusion of theoretical uncertainties. For the large-angle solution, we find $\chi^2=5.7$ (5.2).

In Fig. 7, theoretical values of the double ratio $R_{\mu/e}/R^0_{\mu/e}$ greater than one are allowed for atmospheric neutrinos, because the atmospheric ν_e's can now oscillate into other flavors, thus increasing $R_{\mu/e}$. The region allowed by the atmospheric neutrino data (whose best-fit point is represented by the small circle) is then pushed towards higher values of ψ. Moreover, for accelerator and reactor neutrinos all the experimental bounds can be mapped into the plane $(s^2_{2\psi}, m^2_3)$ (except for IRP, which puts no limits at $\sin^2\phi=0.1 \Longleftrightarrow \sin^2 2\phi=0.36$). Remarkably, the Gösgen experiment, which measures $P(\nu_e \to \nu_e)$, gives rise to the dominant bound independently of the angle ψ, as explained in Sec. III, and excludes a large part of the previous region. Only a small zone survives, around $m^2_3 \simeq 10^{-2}$ eV^2 at large $\sin^2 2\psi$. The χ^2 value at the minimum, for the atmospheric neutrino data only, is 4.53 (4.45) without (with) the inclusion of the theoretical errors. Thus, the minimum solar+atmospheric χ^2 is 6.01 (5.77), slightly higher than in the $\phi=0$ case.

Finally, we note again that assumption (7) is satisfied at almost the 3σ level by the final solutions reported in Figs. 6 and 7.

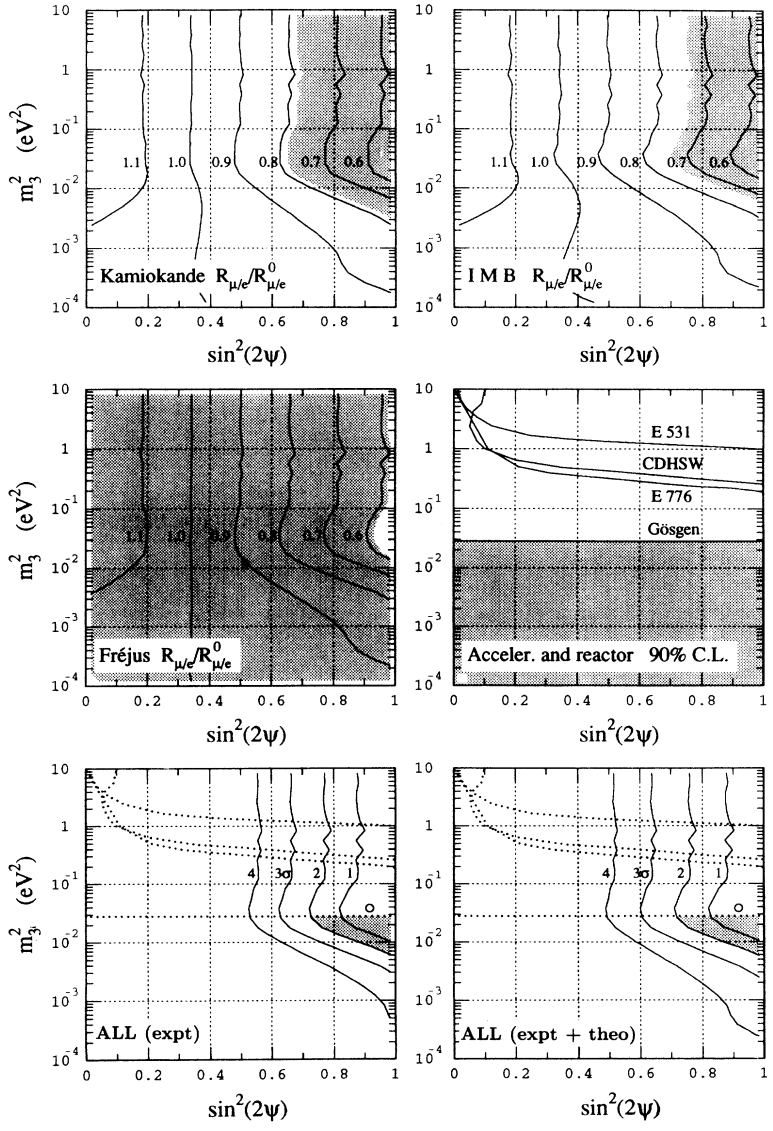

FIG. 7. As in Fig. 5, but for $s^2_\phi=0.1$.

C. $\sin^2\phi=0.25$

The trend emerging in the comparison of the previous two cases is enhanced for such a large mixing ($\sin^2\phi=0.25 \Longleftrightarrow \sin^2 2\phi=0.75$) between the first and the third generations.

In Fig. 8 the broadening and shifting of the allowed regions are evident. At the 3σ level (or more) the small-angle and the large-angle solutions merge into a single one, spanning a large part of the plane. The χ^2 values for the small- and large-angle solutions are 3.30 and 6.8 (3.18, 6.5) without (with) the inclusion of the theoretical uncertainties.

In Fig. 9 the most striking result is that the IRP bound is probed, which exactly excludes the zone allowed at the 2σ level by the combined atmospheric neutrino data. This scenario is thus highly disfavored. Considering only the atmospheric neutrino data, the χ^2 at the minimum is 4.95 (4.94) without (with) the inclusion of the theoretical flux uncertainties. This translates into a minimum solar+atmospheric $\chi^2=8.25$ (8.12), about three units higher than for $\phi=0$. This corroborates the statement that the scenario with $\sin^2\phi=0.25$ is disfavored.

Our assumption (7) is here satisfied at the 2σ level, and for a large part of the 3σ-allowed region. For larger values of $\sin^2\phi$, the IRP bound would be (slightly) stronger and the total χ^2 higher. Thus, the value 0.25 can be considered (at least) a 2σ upper bound on $\sin^2\phi$.

VII. CONCLUSIONS AND PROSPECTS

Assuming neutrino oscillations as the most natural available solution to both the "solar neutrino problem" and the "atmospheric neutrino anomaly," we have presented a comprehensive analysis of the solar and atmospheric neutrino data (except for upward-going muons) in a three-generation scheme, including the limits induced by the reactor and accelerator experiments.

In order to simplify the hard problem of a three-

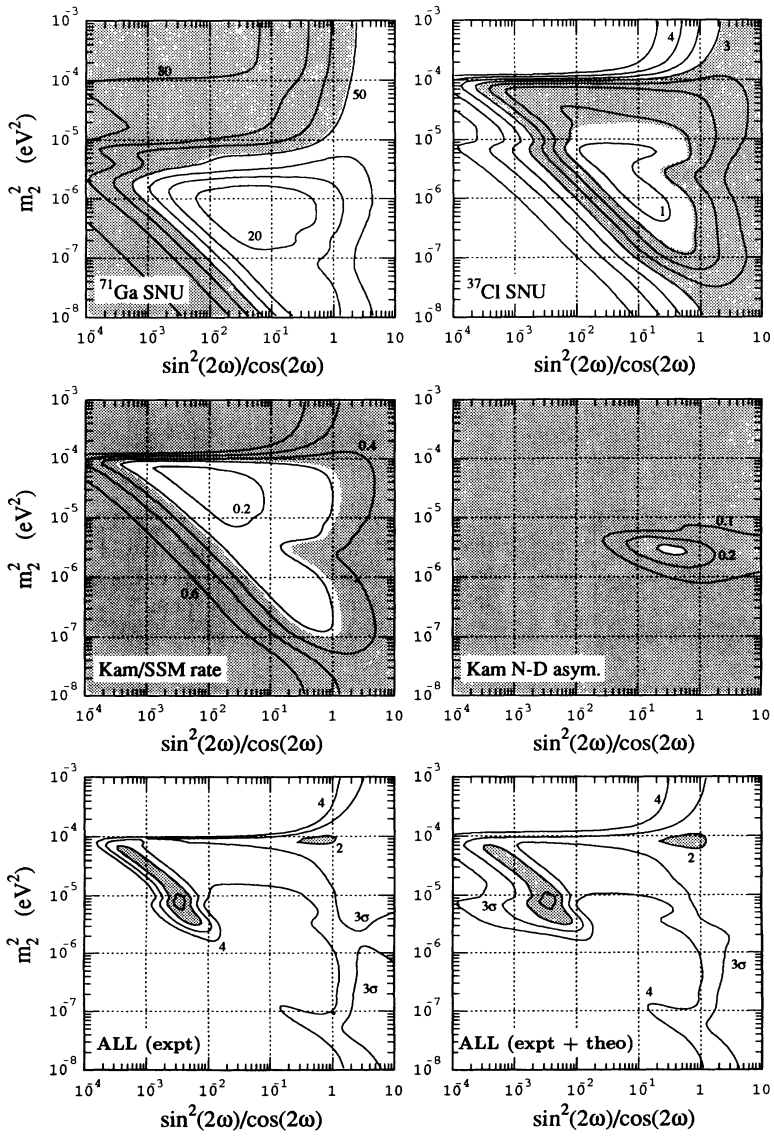

FIG. 8. As in Fig. 4, but for $s^2_\phi=0.25$.

generation description, a natural mass hierarchy has been assumed, consistently derived by considering the present limits of solar and atmospheric neutrino experiments. Within this hierarchical scheme, we have "translated," for the first time, the present experimental information coming from solar, atmospheric, reactor, and accelerator neutrinos into a set of combined limits on the five relevant parameters $m_2^2, m_3^2, \omega, \psi, \phi$. In particular, we were able to constrain m_2^2 and ω in well-defined regions. We have also set lower bounds on ψ, an upper bound on ϕ, and both a lower and an upper bound on m_3^2. The final allowed mass ranges have been shown to lie well within the limits preliminarly assumed, so ensuring the self-consistency of our hierarchical scenario.

In the analysis of the solar neutrino data, the Earth regeneration effect and the inclusion of the theoretical errors have proven to be crucial, in particular in the determination of the large-angle solution. In the analysis of the atmospheric neutrino data, we have considered the three most important experiments, Kamiokande, IMB, and Fréjus, and have consistently included the atmospheric neutrino fluxes, treating their uncertainties as a common systematic error affecting the three experiments. We consider such a treatment of the atmospheric flux errors as a noteworthy point of our approach: even though, at present, these uncertainties cannot be considered as crucial, we expect the point to become more and more relevant with the improvement of the experimental precision. We plan to treat in a future paper matter effects on atmospheric neutrinos traversing the Earth, since they might require the inclusion of the subleading oscillation, here neglected.

As far as the mixing angles are concerned, the naïve expectation (or theoretical prejudice) $\phi < \psi < \omega$, can only be satisfied by choosing the (disfavored) large-angle solution for ω. It is worth noting, however, that the popular seesaw mechanism [72], which naturally predicts $m_1^2 < m_2^2 < m_3^2$, does not necessarily force the neutrino

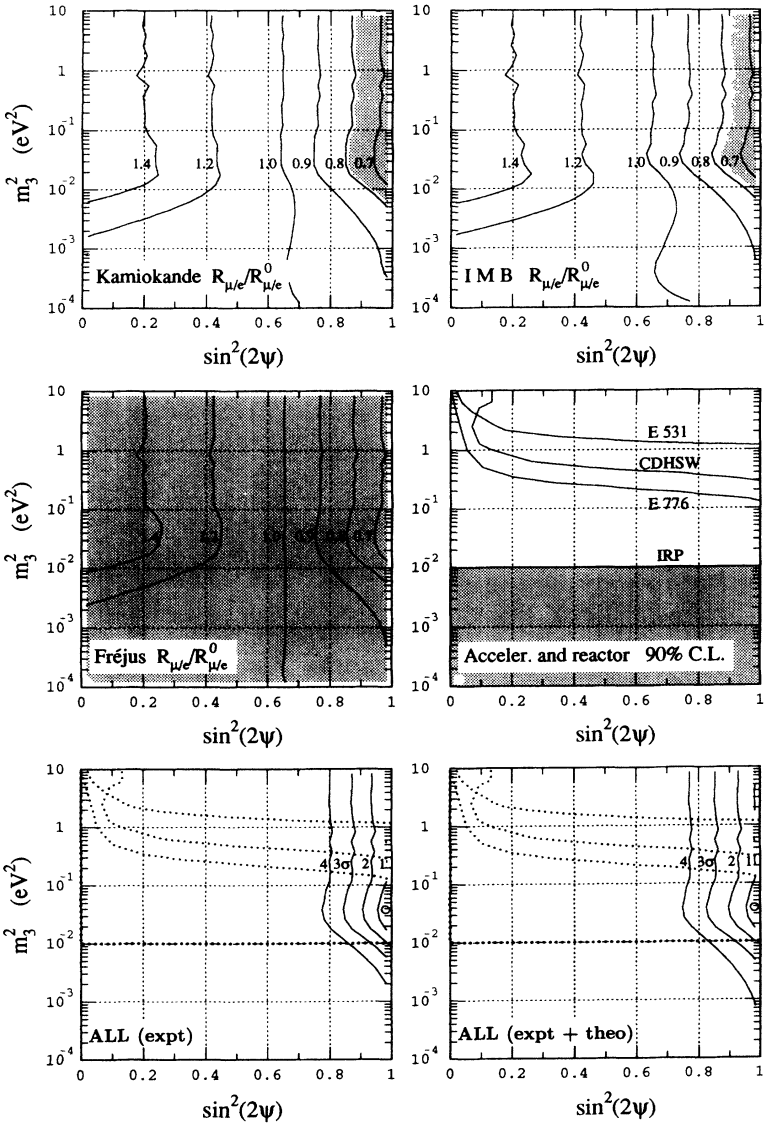

FIG. 9. As in Fig. 5, but for $s_\phi^2 = 0.25$. Notice that at the 2σ level the allowed region (compatible with the IRP limit) in the last two subfigures shrinks to the "point" $(s_{2\psi}^2, m_3^2) = (1, 10^{-2}\ \text{eV}^2)$.

mixing angles to be small and hierarchical as in the quark sector [73], [74].

The combined limits that we have obtained, although already impressive, will certainly be improved in the near future. On-going solar and atmospheric neutrino experiments are expected to reduce not only the statistical but also the systematic errors. This would allow us to refine the present analysis both for atmospheric neutrinos (including the whole set of contained events and possibly also the upward-going muons) and for accelerator and reactor neutrinos (analyzing the raw experimental data). However, it is likely that only the next generation of neutrino oscillation experiments (a recent presentation is given in Ref. [75]) will have a definite word on the mass and mixing scenario analyzed in this paper, and will eliminate the ambiguities that now allow different interpretations of the data.

In particular, future solar neutrino experiments are expected to select, at a very high confidence level, one of two solutions in the plane $(s^2_{2\omega}/c_{2\omega}, m^2_2)$. New atmospheric data will help in constraining m^2_3 from below, narrowing the allowed range of $s^2_{2\psi}$. Future reactor neutrino experiments could not only improve the combined bounds on $s^2_{2\phi}$ and m^2_3 but, together with the atmospheric neutrino results, strengthen the absolute upper bound on ϕ, as we have shown. For very low values of ϕ, accelerator experiments in the channels $(\nu_\mu \to \nu_\mu)$ and $(\nu_\mu \to \nu_\tau)$ will extend the explored region in the plane $(s^2_{2\psi}, m^2_3)$. The channel $(\nu_\mu \to \nu_e)$, and possibly $(\nu_e \to \nu_\tau)$, will be complementary probes for relatively high values of ϕ.

Any unmistakable evidence for neutrino oscillations in one of these experimental sectors is constrained to have effects on the others, and only a comprehensive analysis in the parameter space $(m^2_2, m^2_3, \omega, \phi, \psi)$, such as the one presented in this paper, is able to point out all the connections existing among the different pieces of data.

ACKNOWLEDGMENTS

One of us (E.L.) would like to thank the CERN Theory Division for its kind hospitality during the preparation and completion of this work.

[1] Gargamelle Collaboration, F. J. Hasert *et al.*, Phys. Lett. **46B**, 138 (1973); Nucl. Phys. B **73**, 1 (1974).
[2] R. Davis, Jr., in *Proceedings of the 21st International Cosmic Ray Conference,* Adelaide, Australia, 1989, edited by R. J. Protheroe (University of Adelaide Press, Adelaide, 1990), Vol. 12, p. 143.
[3] Kamiokande Collaboration, K. S. Hirata *et al.*, Phys. Rev. Lett. **65**, 1297 (1990); Phys. Rev. D **44**, 2241 (1991); presented by T. Kajita, in *Proceedings of the 26th International Conference on High Energy Physics,* Dallas, Texas, 1992, edited by J. Sanford, AIP Conf. Proc. No. 272 (AIP, New York, 1993).
[4] GALLEX Collaboration, P. Anselmann *et al.*, Phys. Lett. B **285**, 376 (1992); presented by D. Vignaud, in *Proceedings of the 26th International Conference on High Energy Physics* [3].
[5] GALLEX Collaboration, presented by F. von Feilitzsch, in *Proceedings of the International Conference "Neutral Currents Twenty Years Later,"* Paris, 1993 (in press).
[6] SAGE Collaboration, A. I. Abazov *et al.*, Phys. Rev. Lett. **67**, 3332 (1991); presented by A. Gavrin, in *Proceedings of the 26th International Conference on High Energy Physics* [3].
[7] J. N. Bahcall, W. F. Huebner, S. H. Lubow, P. D. Parker, and R. K. Ulrich, Rev. Mod. Phys. **54**, 767 (1982).
[8] J. N. Bahcall and R. K. Ulrich, Rev. Mod. Phys. **60**, 297 (1988).
[9] J. N. Bahcall and M. H. Pinsonneault, Rev. Mod. Phys. **64**, 885 (1992).
[10] L. Wolfenstein, Phys. Rev. D **17**, 2369 (1978).
[11] S. P. Mikheyev and A. Yu. Smirnov, Yad. Fiz. **42**, 1441 (1985) [Sov. J. Nucl. Phys. **42**, 913 (1985)].
[12] T. K. Kuo and J. Pantaleone, Rev. Mod. Phys. **61**, 937 (1989).
[13] Kamiokande Collaboration, K. S. Hirata *et al.*, Phys. Lett. B **280**, 146 (1992).
[14] IMB Collaboration, D. Casper *et al.*, Phys. Rev. Lett. **66**, 2561 (1991).
[15] IMB Collaboration, R. Becker-Szendy *et al.*, Phys. Rev. D **46**, 3720 (1992).
[16] Fréjus Collaboration, Ch. Berger *et al.*, Phys. Lett. B **227**, 489 (1989).
[17] NUSEX Collaboration, M. Aglietta *et al.*, Europhys. Lett. **8**, 611 (1989).
[18] Y. Totsuka, in *Neutrino '92,* Proceedings of the Twenty-Fifth International Conference on Neutrino Physics and Astrophysics, Granada, Spain, 1992, edited by A. Morales [Nucl. Phys. B (Proc. Suppl.) **31**, 428 (1993)].
[19] E. V. Bugaev and V. A. Naumov, Phys. Lett. B **232**, 391 (1989).
[20] W. A. Mann, T. Kafka, and W. Leeson, Phys. Lett. B **291**, 200 (1992).
[21] Soudan 2 Collaboration, W. W. Allison *et al.* (unpublished).
[22] G. S. Abrams *et al.*, Phys. Rev. Lett. **63**, 2173 (1989).
[23] The LEP Collaborations: ALEPH, DELPHI, L3, and OPAL, Phys. Lett. B **276**, 247 (1992).
[24] Kamiokande Collaboration, K. S. Hirata *et al.*, Phys. Rev. Lett. **66**, 9 (1991).
[25] T. K. Kuo and J. Pantaleone, Phys. Rev. D **35**, 3432 (1987).
[26] H. Harari and M. Leurer, Phys. Lett. B **181**, 123 (1986).
[27] V. Barger, K. Wishnant, and R. J. N. Phillips, Phys. Rev. Lett. **45**, 2084 (1980).
[28] T. K. Kuo and J. Pantaleone, Phys. Lett. B **198**, 406 (1987).
[29] GALLEX Collaboration, P. Anselmann *et al.*, Phys. Lett. B **285**, 390 (1992).
[30] S. A. Bludman, H. Hata, D. C. Kennedy, and P. G. Langacker, Phys. Rev. D **47**, 2220 (1993).
[31] G. L. Fogli and E. Lisi, Astropart. Phys. (to be published).
[32] V. Barger, K. Wishnant, D. Cline, and R. J. N. Phillips, Phys. Lett. **93B**, 195 (1980); J. Phys. G **6**, L165 (1980); V. Barger, K. Wishnant, and R. J. N. Phillips, Phys. Rev. D **22**, 1636 (1980).
[33] V. Barger and K. Wishnant, Phys. Lett. B **209**, 365 (1988).

[34] K. Hidaka, M. Honda, and S. Midorikawa, Phys. Rev. Lett. **61**, 1537 (1988).
[35] S. Midorikawa, M. Honda, and K. Kasahara, Phys. Rev. D **44**, 3379 (1991).
[36] L. Oberauer and F. van Feilitzsch, Rep. Prog. Phys. **55**, 1093 (1992).
[37] G. Zaceck *et al.*, Phys. Rev. D **34**, 2621 (1986).
[38] G. S. Vidyakin *et al.*, Zh. Eksp. Teor. Fiz. **98**, 764 (1990) [Sov. Phys. JETP **71**, 424 (1990)].
[39] E776 Collaboration, L. Borodovsky *et al.*, Phys. Rev. Lett. **68**, 274 (1992).
[40] E531 Collaboration, N. Ushida *et al.*, Phys. Rev. Lett. **57**, 2898 (1986).
[41] CDHSW Collaboration, F. Dydak *et al.*, Phys. Lett. B **134**, 281 (1984).
[42] H. Blümer and K. Kleinknecht, Phys. Lett. B **161**, 407 (1985).
[43] A. De Rújula, M. Lusignoli, L. Maiani, S. T. Petcov, and R. Petronzio, Nucl. Phys. B **168**, 54 (1980).
[44] T. K. Kuo and J. Pantaleone, Phys. Rev. Lett. **57**, 1805 (1986).
[45] A. Yu. Smirnov, in *Proceedings of the 7th Moriond Workshop on "New and Exotic Phenomena,"* Les Arcs, 1987, edited by O. Fackler and J. Trân Thanh Vân (Frontières, Paris, 1987), p. 275; C. W. Kim, S. Nussinov, and W. K. Sze, Phys. Lett. B **184**, 403 (1987); S. Toshev, Phys. Lett. B **185**, 177 (1987); **192**, 478(E) (1987); A. Baldini and G. F. Giudice, *ibid.* **186**, 211 (1987); S. T. Petcov and S. Toshev, *ibid.* **187**, 120 (1987); H. W. Zaglauer and K. H. Schwarzer, *ibid.* **198**, 556 (1987); Z. Phys. C **40**, 273 (1988); S. P. Mikheyev and A. Yu. Smirnov, Phys. Lett. B **200**, 560 (1988); S. T. Petcov, *ibid.* **214**, 259 (1988).
[46] D. Harley, T. K. Kuo, and J. Pantaleone, Phys. Rev. D **47**, 4059 (1993); (unpublished).
[47] X. Shi and D. N. Schramm, Phys. Lett. B **283**, 305 (1992); X. Shi, D. N. Schramm, and J. N. Bahcall, Phys. Rev. Lett. **69**, 717 (1992).
[48] D. L. Anderson, *Theory of the Earth* (Blackwell, Boston, 1989).
[49] J. Bouchez, M. Cribier, W. Hampel, J. Rich, M. Spiro, and D. Vignaud, Z. Phys. C **32**, 499 (1986); M. Cribier, W. Hampel, J. Rich, and D. Vignaud, Phys. Lett. B **182**, 89 (1986).
[50] A. J. Baltz and J. Weneser, Phys. Rev. D **35**, 528 (1987); **37**, 3364 (1988).
[51] S. Hiroi, H. Sakuma, T. Yanagida, and M. Yoshimura, Prog. Theor. Phys. **78**, 1428 (1987).
[52] A. Dar and A. Mann, Nature (London) **325**, 790 (1987); A. Dar, A. Mann, Y. Melina, and D. Zajfman, Phys. Rev. D **35**, 3607 (1987).
[53] J. M. LoSecco, Phys. Rev. D **47**, 2032 (1993).
[54] N. Hata and P. Langacker, Phys. Rev. D **48**, 2937 (1993).
[55] T. K. Gaisser, T. Stanev, and G. Barr, Phys. Rev. D **38**, 85 (1988); G. Barr, T. K. Gaisser, and T. Stanev, *ibid.* **39**, 3532 (1989).
[56] M. Honda, K. Kasahara, K. Hidaka, and S. Midorikawa, Phys. Lett. B **248**, 193 (1990).
[57] H. Lee and Y. S. Koh, Nuovo Cimento **105B**, 883 (1990).
[58] L. V. Volkova, in *Cosmic Gamma Rays, Neutrinos and Related Astrophysics,* edited by M. M. Shapiro and J. P. Wefel, Proceedings of the NATO Advanced Study Institute, NATO ASI series B: Physics, Vol. 270, edited by M. M. Shapiro and J. P. Wefel (Plenum, New York, 1989), p. 139.
[59] D. H. Perkins, Nucl. Phys. B **399**, 3 (1993).
[60] M. M. Boliev *et al.*, in *Proceedings of the 3rd International Workshop on Neutrino Telescopes,* Venice, 1991, edited by M. Baldo Ceolin (Università, Padua, 1991), p. 235.
[61] Y. Oyama *et al.*, Phys. Rev. D **39**, 1481 (1989).
[62] IMB Collaboration, R. Becker-Szendy *et al.*, Phys. Rev. Lett. **69**, 1010 (1992).
[63] W. Frati, T. K. Gaisser, A. K. Mann, and T. Stanev, Phys. Rev. D **48**, 1140 (1993).
[64] E. D. Carlson, Phys. Rev. D **34**, 1454 (1986).
[65] C. Llewellyn Smith, Phys. Rep. C **3**, 261 (1972).
[66] M. Nakahata *et al.*, J. Phys. Soc. Jpn. **55**, 3786 (1986).
[67] G. L. Fogli and G. Nardulli, Nucl. Phys. B **160**, 116 (1979).
[68] A. Suzuki, in *Neutrino '88,* Proceedings of the 13th International Conference on Neutrino Physics and Astrophysics, Boston, Massachusetts, 1988, edited by J. Schneps, T. Kafka, W. A. Mann, and P. Nath (World Scientific, Singapore, 1989), p. 631.
[69] Kamiokande Collaboration, K. S. Hirata *et al.*, Phys. Lett. B **205**, 417 (1988).
[70] E. W. Beier *et al.*, Phys. Lett. B **283**, 446 (1992).
[71] Fréjus Collaboration, Ch. Berger *et al.*, Phys. Lett. B **245**, 305 (1990).
[72] M. Gell-Mann, P. Ramond, and R. Slansky, in *Supergravity,* Proceedings of the Workshop, Stony Brook, New York, 1979, edited by P. van Nieuwenhuizen and D. Freedman (North-Holland, Amsterdam, 1979), p. 315.
[73] A. Yu. Smirnov, Phys. Rev. D **48**, 3264 (1993).
[74] C. H. Albright, Phys. Rev. D **43**, R3595 (1991); **45**, R725 (1992).
[75] J. P. Revol, presented at *Les Rencontres de Physique de la Vallee d'Aoste,* La Thuile, 1993, edited by M. Greco (Frontières, Gif-sur-Yvette, 1993), p. 61.

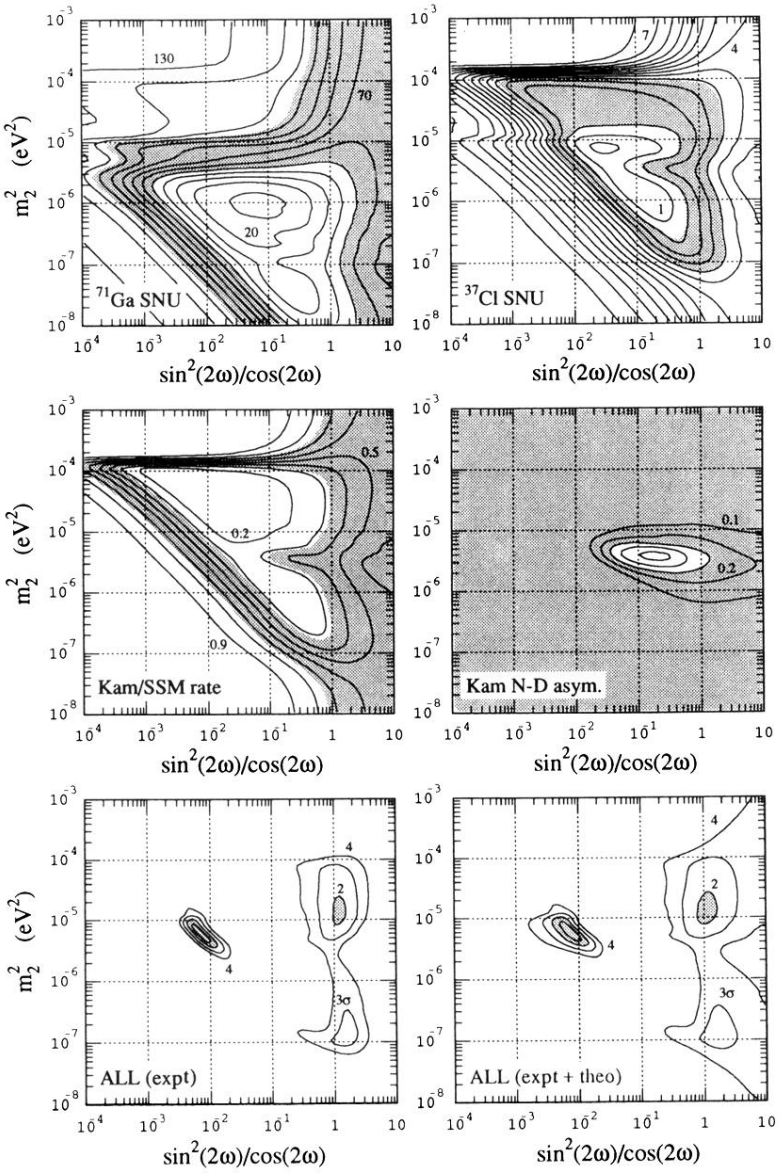

FIG. 4. MSW solutions to the solar neutrino problem for $s_\phi^2 = 0$. The grey areas, allowed at the 2σ level, refer to each experiment separately in the upper four subfigures, and to their combination in the lower two (ALL). See the text for details.

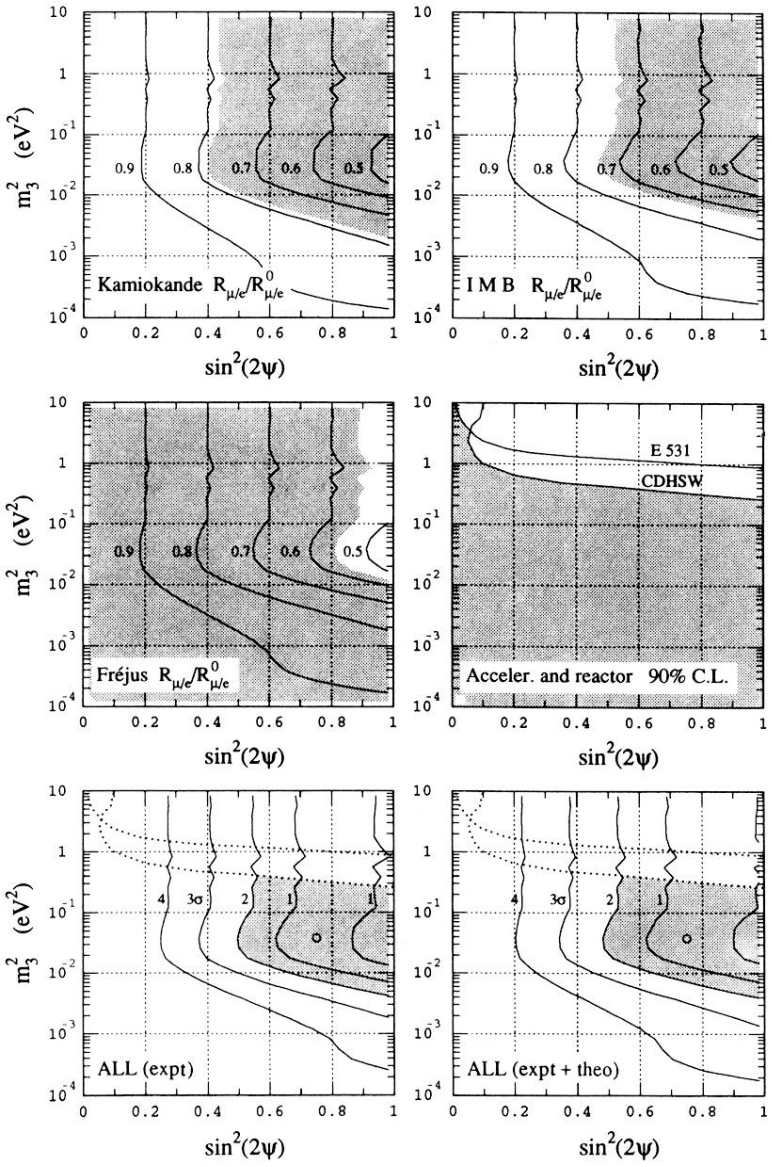

FIG. 5. Vacuum oscillation solutions to the atmospheric neutrino deficit for $s^2_\phi = 0$, compared with the accelerator and reactor limits. The grey areas are allowed at the 2σ level (or 90%, where indicated). The combined bounds are shown in the last two subfigures (ALL). See the text for details.

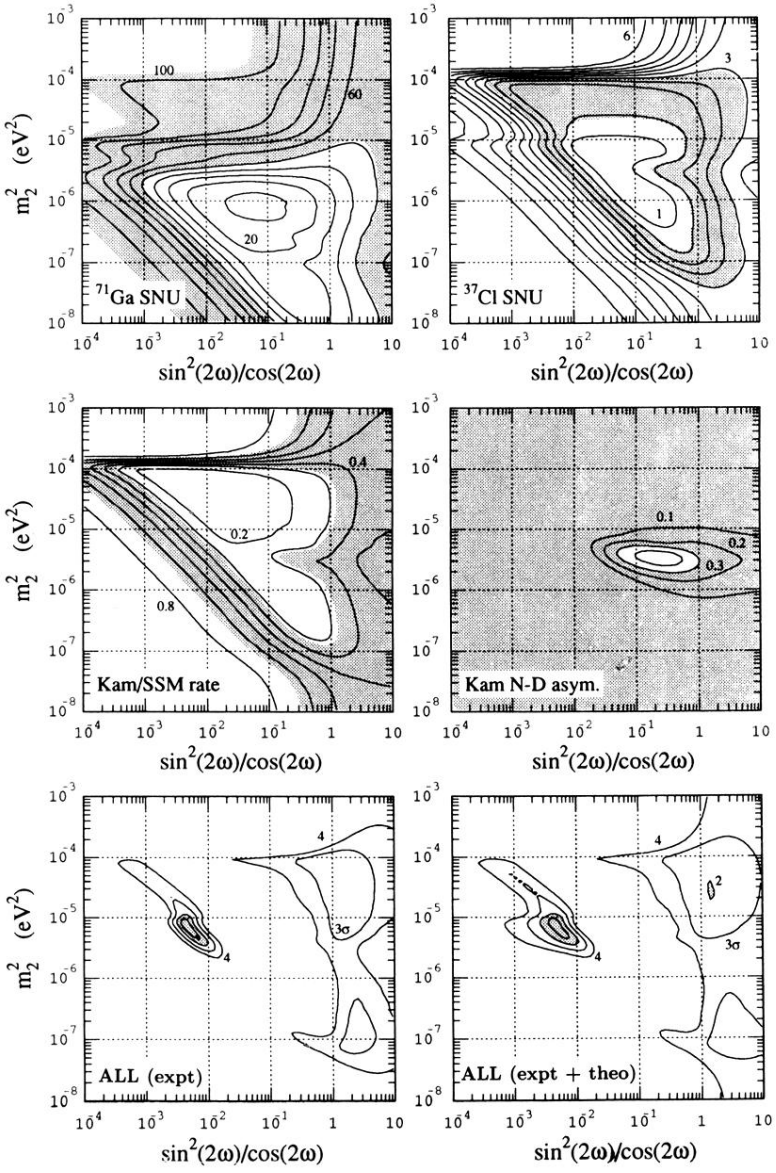

FIG. 6. As in Fig. 4, but for $s_\phi^2 = 0.1$.

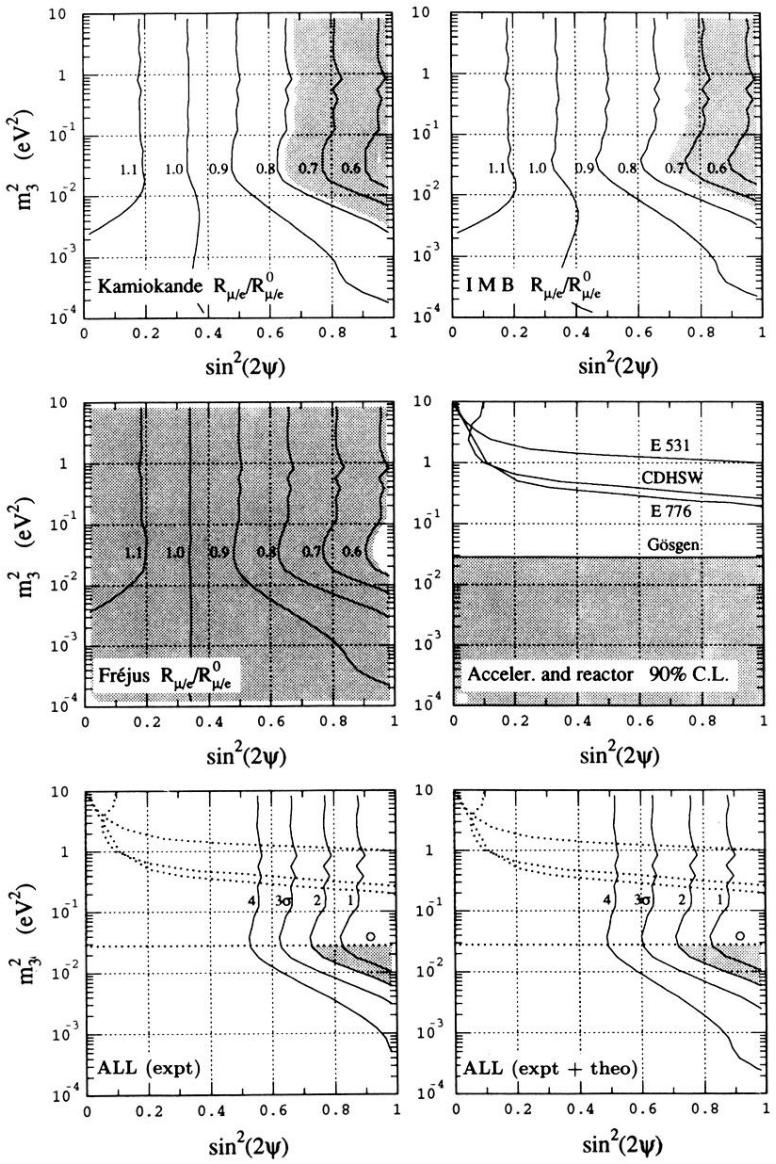

FIG. 7. As in Fig. 5, but for $s^2_\phi = 0.1$.

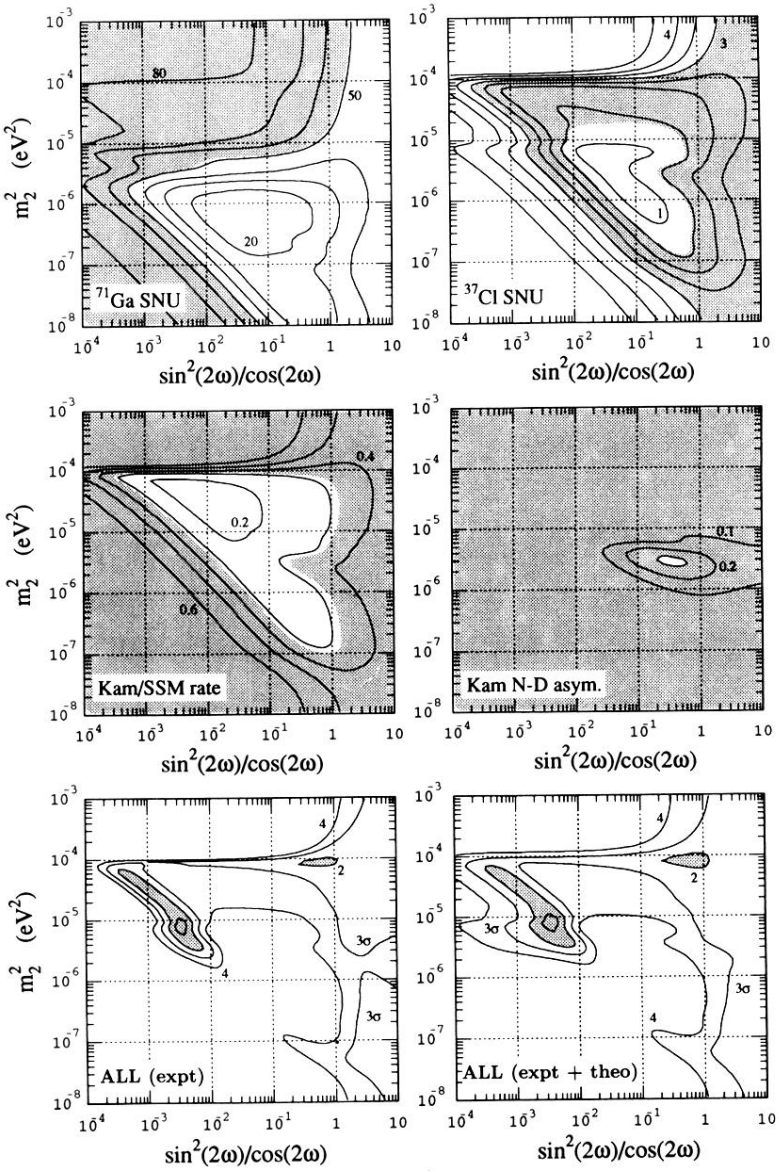

FIG. 8. As in Fig. 4, but for $s_\phi^2 = 0.25$.

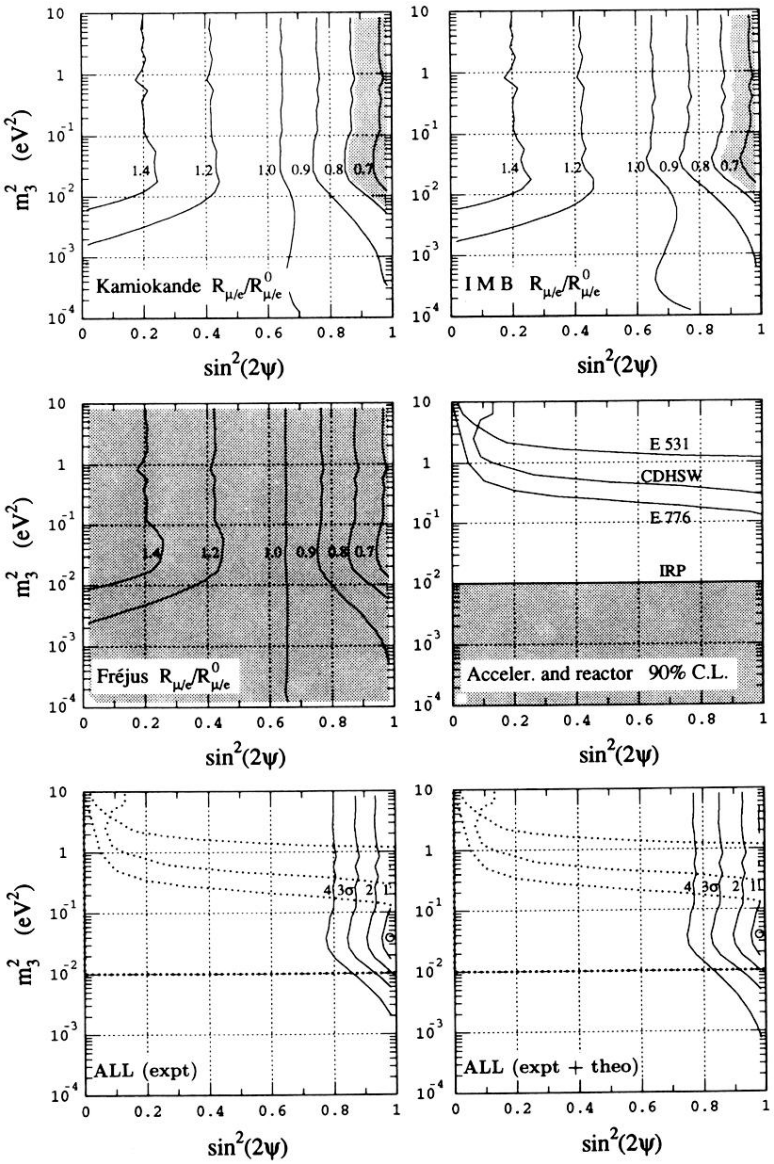

FIG. 9. As in Fig. 5, but for $s^2_\phi = 0.25$. Notice that at the 2σ level the allowed region (compatible with the IRP limit) in the last two subfigures shrinks to the "point" $(s^2_{2\psi}, m^2_3) = (1, 10^{-2}\,\text{eV}^2)$.